Acta Pharmaceutica Sinica B 2023;13(2):598–617

Chinese Pharmaceutical Association
Institute of Materia Medica, Chinese Academy of Medical Sciences

Acta Pharmaceutica Sinica B

www.elsevier.com/locate/apsb
www.sciencedirect.com

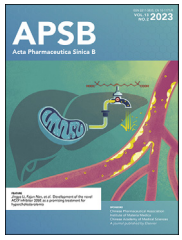

ORIGINAL ARTICLE

Heliangin acts as a covalent ligand of RPS2 that disrupts pre-rRNA metabolic processes in *NPM1*-mutated acute myeloid leukemia

Yin Feng[a,b,†], Yefan Han[a,b,†], Anni Hu[a,b], Yi Qu[a,b], Yili Hu[c], Hao Wu[a], Xinzhi Wang[a,b,*], Li He[d,*]

[a]*College of Pharmacy, Nanjing University of Chinese Medicine, Nanjing 210046, China*
[b]*China Jiangsu Key Laboratory of Research and Development in Marine Bio-resource Pharmaceutics, Nanjing 210046, China*
[c]*Experiment Center for Science and Technology, Nanjing University of Chinese Medicine, Nanjing 210046, China*
[d]*Department of Hematology, Zhongnan Hospital of Wuhan University, Wuhan 430071, China*

Received 11 April 2022; received in revised form 5 July 2022; accepted 23 September 2022

KEY WORDS

Acute myeloid leukemia;
Heliangin;
NPM1-mutation;
Differentiation;
Pre-rRNA;
Covalent;
RPS2;
p53 stabilization

Abstract Although *NPM1* mutations are frequently found in acute myeloid leukemia patients, therapeutic strategies are scarce and unsuitable for those who cannot tolerate intensive chemotherapy. Here we demonstrated that heliangin, a natural sesquiterpene lactone, exerts favorable therapeutic responses in *NPM1* mutant acute myeloid leukemia cells, with no apparent toxicity to normal hematogenous cells, by inhibiting their proliferation, inducing apoptosis, causing cell cycle arrest, and promoting differentiation. In-depth studies on its mode of action using quantitative thiol reactivity platform screening and subsequent molecular biology validation showed that the ribosomal protein S2 (RPS2) is the main target of heliangin in treating *NPM1* mutant AML. Upon covalent binding to the C222 site of RPS2, the electrophilic moieties of heliangin disrupt pre-rRNA metabolic processes, leading to nucleolar stress, which in turn regulates the ribosomal proteins−MDM2−p53 pathway and stabilizes p53. Clinical data shows that the pre-rRNA metabolic pathway is dysregulated in acute myeloid leukemia patients with the *NPM1* mutation, leading to a poor prognosis. We found that RPS2 plays a critical role in regulating this pathway and may be a novel treatment target. Our findings suggest a novel treatment strategy and lead compound for acute myeloid leukemia patients, especially those with *NPM1* mutations.

*Corresponding authors.
E-mail addresses: xinzhiwang@njucm.edu.cn (Xinzhi Wang), lihe126@whu.edu.com (Li He).
[†]These authors made equal contributions to this work.
Peer review under responsibility of Chinese Pharmaceutical Association and Institute of Materia Medica, Chinese Academy of Medical Sciences.

https://doi.org/10.1016/j.apsb.2022.10.018
2211-3835 © 2023 Chinese Pharmaceutical Association and Institute of Materia Medica, Chinese Academy of Medical Sciences. Production and hosting by Elsevier B.V. This is an open access article under the CC BY-NC-ND license (http://creativecommons.org/licenses/by-nc-nd/4.0/).

© 2023 Chinese Pharmaceutical Association and Institute of Materia Medica, Chinese Academy of Medical Sciences. Production and hosting by Elsevier B.V. This is an open access article under the CC BY-NC-ND license (http://creativecommons.org/licenses/by-nc-nd/4.0/).

1. Introduction

Acute myeloid leukemia (AML) is a common blood cancer characterized by rapid infiltration of the patient's bone marrow, blood, or other tissues by abnormally proliferating, poorly differentiated myeloid hematopoietic cells[1,2]. The cure rate of AML is highly correlated with patient age and is approximately 35%−40% for patients aged ≤60 years, and 5%−15% for patients aged >60 years[1−3]. The clinical treatment of AML patients has not changed substantially in over 30 years, with intensive induction chemotherapy being the preferred option. This primarily consists of treatment with intravenous anthracyclines for three days and continuous injections of cytarabine for seven days[4]. However, most patients aged >60 years cannot receive this treatment for safety reasons or require a lower dose to reduce the side effects caused by chemotherapy. This leads to poor outcomes in this group, with a median survival of only 5 months[1]. Although the genetic abnormalities that contribute to AML have been well studied for many years, and the importance of these abnormalities in the prognosis of AML is widely accepted, the targeting of these molecules with appropriate clinical treatments is still in its early stages[5]. Among these, the nucleophosmin 1 (*NPM1*) mutation is found frequently in AML patients, accounting for approximately 25%−35% of all cases. The mutated *NPM1* gene has an insertion in the terminal exon, resulting in the loss of nuclear localization and the generation of a new nuclear export signal. Thus, in contrast with the wild-type (WT) NPM1 protein which is localized in the nucleus, the mutant protein is abnormally localized in the cytoplasm (NPM1c) where it inhibits the normal function of key nuclear proteins (*e.g.*, tumor suppressors and transcription factors) by binding and exporting them to the cytoplasm, thereby causing AML[6−9]. Currently, no targeted therapy exists for the treatment of AML caused by the *NPM1* mutation. Although an exportin-1 (XPO1) inhibitor that targets the abnormal export of NPM1c protein has recently been developed[10], it is still in the early stages of a clinical study (NCT02649790). Clinical treatment of this type of AML is currently limited to conventional chemotherapy, which is not feasible for most patients aged >60 years[7]. Therefore, it is crucial to develop new targeted treatments and more sensitive drugs that are less toxic.

Jerusalem artichoke (*Helianthus tuberosus* L.) is an annual perennial herb belonging to the family Asteraceae[11]. Owing to its salt and drought tolerance, it has recently been cultivated in saline soils and coastal tidal flats throughout China for soil salinity control and ecological improvement. The underground tuber of this plant is rich in inulin and is currently used for industrial and food purposes. However, the aerial stem and leaves are often discarded or used only as livestock feed. Chemical studies have shown that the main constituents of the Jerusalem artichoke are heliangolide-type sesquiterpene lactones[12−14]. As reported in the literature, sesquiterpene lactones isolated from this plant contains the α-methylene-γ-butyrolactone group, which is a typical covalent ligand[15]. It is well known that sesquiterpene lactones with this bioactive group have anti-inflammatory and antitumor activities. The electrophilic group can covalently bind to cysteine residues in certain protein targets, thus exerting its corresponding physiological activity[16−23]. In our previous study, we found that heliangin (HEL), a representative component of heliangolides, elicited sensitivity in hematological tumors, especially in *NPM1* mutant AML[24]. This compound not only significantly inhibited the proliferation of *NPM1* mutant AML cells and promoted their differentiation into normal blood cells, but also had no significant toxicity to normal hematopoietic cells, suggesting that it could be a novel lead compound for treating *NPM1* mutant AML. However, the underlying mechanism and target of this compound in treating *NPM1* mutant AML are not yet known; this information is needed to structurally modify and further develop HEL as a drug lead. In addition, elucidating the drug target will enable the development of targeted drugs based on the identification of novel therapeutic targets. This is of particular importance for the treatment of patients aged >60 years suffering from this disease.

Recently, mass spectrometry-based isoTOP-ABPP techniques have made a rapid search for covalent ligand small-molecule protein targets and binding sites possible[25]. Using this approach, laboratories worldwide have screened for and obtained novel covalently binding drug targets of multiple bioactive natural products[26−28]. Quantitative thiol reactivity profiling (QTRP), which was introduced in 2020, is the latest generation of this technique[29]. This method involves extensive labeling of reactive cysteines in cell and tissue samples (*e.g.*, control *vs.* treatment) by a 2-iodo-*N*-(prop-2-yn-1-yl)acetamide (IPM) probe that is electrophilically bound to sulfhydryl groups, which are then processed into tryptic peptides and tagged by click chemistry with an isotopically labeled azido-biotin reagent containing a photocleavable linker. Biotin-binding peptides are then captured with streptavidin beads, and mass spectrometry-based shotgun proteomics is applied to identify and quantify the photo-released peptide. Finally, the mass spectrometry data are analyzed using proteomics software to determine the covalent protein target and binding site. Compared with conventional isoTOP-ABPP, this new technique has the advantages of fast sample processing time, short mass spectrometry analysis time, high sensitivity, and good accuracy.

In this study, we focused on further evaluating the effect of HEL *in vitro* and *in vivo* using RNA-seq, QTRP, and other omics technologies to screen the anti-*NPM1* mutant AML pathway and target. The pathways and targets obtained from screening were validated using multiple molecular biology methods. The ultimate goal of this study was to provide a basis for further development of this lead molecule and to provide new methods for targeted therapy of *NPM1* mutant AML patients.

2. Materials and methods

2.1. Ethical statement

All animal studies were conducted in strict accordance with the recommendations of the Guidelines for the Care and Use of Laboratory Animals of the Ministry of Science and Technology of China. The protocol and experimental designs were reviewed and approved by the Animal Ethics Committee of Nanjing University of Chinese Medicine (#202104A02, Nanjing, China). Immunocompromised NOD-*Prkdc*^{scid}*Il2rg*^{em1}/Smoc (M-NSG) male mice were purchased

from the Shanghai Model Organisms Center Inc. (Animal Certificate: SCXK(Hu) 2017-0010; Shanghai, China). Mice were housed under sterile conditions using HEPA-filtered microisolators and fed irradiated food and sterile water. All possible steps were taken to avoid the animals' suffering at any stage of the experiment.

2.2. Chemicals

Heliangin (HEL, CAS# 13,323-48-3) was previously isolated and purified from the stem and leaf parts of *H. tuberosus* L. Its structure (Fig. 1A) has been validated by nuclear magnetic resonance and mass spectrometry (Supporting Information Fig. S1) with a purity of 98% (#19-05-25; Nanjing University of Chinese Medicine). All-*trans* retinoic acid (ATRA; > 99% purity) was obtained from APExBIO (#A8539; Houston, TX, USA). Cytarabine (AraC; > 99% purity) was purchased from Shanghai Yuanye Biotech Co. (#B28038; Shanghai, China). Actinomycin D (ActD; > 98% purity) was obtained from GLPBIO (#GC16866; Montclair, CA, USA).

2.3. Cell culture

OCI-AML3 cells (German Collection of Microorganisms and Cell Cultures [DSMZ], Braunschweig, Germany) were cultured in RPMI 1640 medium (#01-100-1ACS; Biological Industries; Kibbutz Beit-Haemek, Israel) containing 20% fetal bovine serum (FBS) (#10270-106; Gibco, Waltham, MA, USA). OCI-AML2 cells (DSMZ) were cultured in MEM-alpha medium (#12561-056, Gibco) containing 20% FBS. U937 (American Type Culture Collection [ATCC], Manassas, VA, USA), HL-60 (ATCC), and THP-1 (ATCC) cells were cultured in RPMI 1640 medium containing 10% FBS. KG-1a cells (ATCC) were cultured in IMDM (#SH30228.01; Hyclone, Logan, UT, USA) supplemented with 20% FBS. Human mesenchymal stem cells (hMSCs, China National Collection of Authentic Cell Cultures [NCACC]) were cultured in a mesenchymal stem cell medium (#7501; ScienCell, Carlsbad, CA, USA) containing 5% FBS. The 293T cell line (ATCC) was cultured in DMEM (#SH30243.01, Hyclone) supplemented with 10% FBS. IMS-M2 cell line was a kind gift from Dr. Li He at Zhongnan Hospital of Wuhan University (Wuhan, China) and cultured in RPMI 1640 medium containing 20% FBS. All cell lines were cultured at 37 °C in a humidified chamber in the presence of 5% CO_2. Penicillin/streptomycin (#SV30010, Hyclone) was added to all cell cultures, except for the medium used for plasmid/siRNA transfection.

2.4. Cell viability assays

Cells were plated at a density of 1.25×10^4 cells per well in 100 μL of medium in a 96-well plate. The next day, cells were treated with 1 μL of either DMSO or HEL to the indicated concentrations and were then incubated at 37 °C in 5% CO_2. After 48 h, cell viability was evaluated using an MTT assay kit (#FMS-MTT01; FCMACS, Nanjing, China) according to the manufacturer's instructions, and absorbance was measured using a Spectra Max i3x (Molecular Devices, San Jose, CA, USA) plate reader. A sample size of $n = 5$ was used for each treatment condition.

2.5. Apoptosis and cell cycle assays

Cells were plated in 6-well plates at a density of 4×10^5/mL and treated for 48 h with either 0.1% DMSO (#D2650, Sigma−Aldrich, St. Louis, MO, USA) or HEL (1, 5, or 10 μmol/L). AraC (5 μmol/L) was used as a positive control.

For cell apoptosis analyses, cells were washed with ice-cold phosphate-buffered saline (PBS) twice and then stained using the Annexin V Alexa Fluor 647 Apoptosis Detection Kit (#FMSAV647-050, FCMACS) according to the manufacturer's instructions, followed by FCM analysis using a Gallios Flow Cytometer (Beckman Coulter, Brea, CA, USA). FlowJo software (v. 10.4) was used to analyze the results. Live cells were defined as annexin$^-$/PI$^-$, and apoptotic cells as annexin$^+$/PI$^-$ or annexin$^+$/PI$^+$.

For cell cycle analyses, the cells were washed twice with ice-cold PBS and then fixed with 70% ethanol at 4 °C overnight. They were then centrifuged at 1000 × *g* for 5 min at 4 °C, and the supernatant was removed. After washing with ice-cold PBS twice, cells were resuspended in 0.5 mL staining buffer containing 50 μg/mL propidium iodide (#40301ES50; Yeasen Biotechnology, Shanghai, China) and 50 μg/mL RNase A (#40301, Yeasen Biotechnology), and analyzed by FCM using the Gallios Flow Cytometer. FlowJo software was used to analyze the results. The sample size was $n = 3$ for each treatment condition.

2.6. Cell differentiation assays

Cell differentiation was detected using the APC-labeled anti-human CD14 (#11-0118-42; eBioscience, San Diego, CA, USA) and FITC or PE-labeled anti-human CD11b (#17-0149-42 or 12-0112-82, eBioscience) antibodies or the corresponding isotype control antibody (FITC-IgG, #11-4714-41, eBioscience; or APC-IgG, #400119, BioLegend, San Diego, CA, USA) and analyzed by FCM.

Cells were plated in 6-well plates at a density of 5×10^5 cells/well and treated for 5 days with either DMSO (0.1%) or HEL (1, 5, or 10 μmol/L). ATRA (1 μmol/L) was used as a positive control. The cell medium was replaced with fresh medium after 3 days of treatment.

For the FCM differentiation assay, cells were washed with ice-cold flow cytometry staining buffer (FCS, #00-4222-26, eBioscience) twice, resuspended in 100 μL FCS buffer, and then stained with FITC-anti-human CD11b or APC-anti-human CD14 for 45 min on ice. Appropriate isotype controls were included in this analysis. After incubation, cells were washed twice with FCS buffer, resuspended in 0.3 mL FCS buffer, and analyzed by FCM using the Gallios Flow Cytometer. FlowJo software was used to analyze the results. The sample size was $n = 3$ for each treatment condition.

2.7. Morphological analysis

Cells were treated as described in section 2.5 for cell differentiation assays. After 5 days of treatment, the cells were centrifuged for 5 min at 1000 × *g* and washed twice with ice-cold PBS. Fifty μL of cells (1×10^4) were dropped onto adherent slides and incubated overnight at 4 °C. Cells were then fixed with methanol for 10 min and stained with Giemsa using the Fast Wright Giemsa kit (#60529ES01, Yeasen Biotechnology) according to the manufacturer's instructions. Images were acquired using an Axio Scope A1 microscope (Zeiss, Jena, Germany).

2.8. In vivo study

M-NSG mice were injected *via* tail vein with 2×10^6 OCI-AML3 cells at 6−9 weeks old. The mice were anesthetized with isoflurane before transplantation. After confirmation of >10% AML bone marrow engraftment in three randomly selected mice, the remaining mice were randomized into groups that were treated

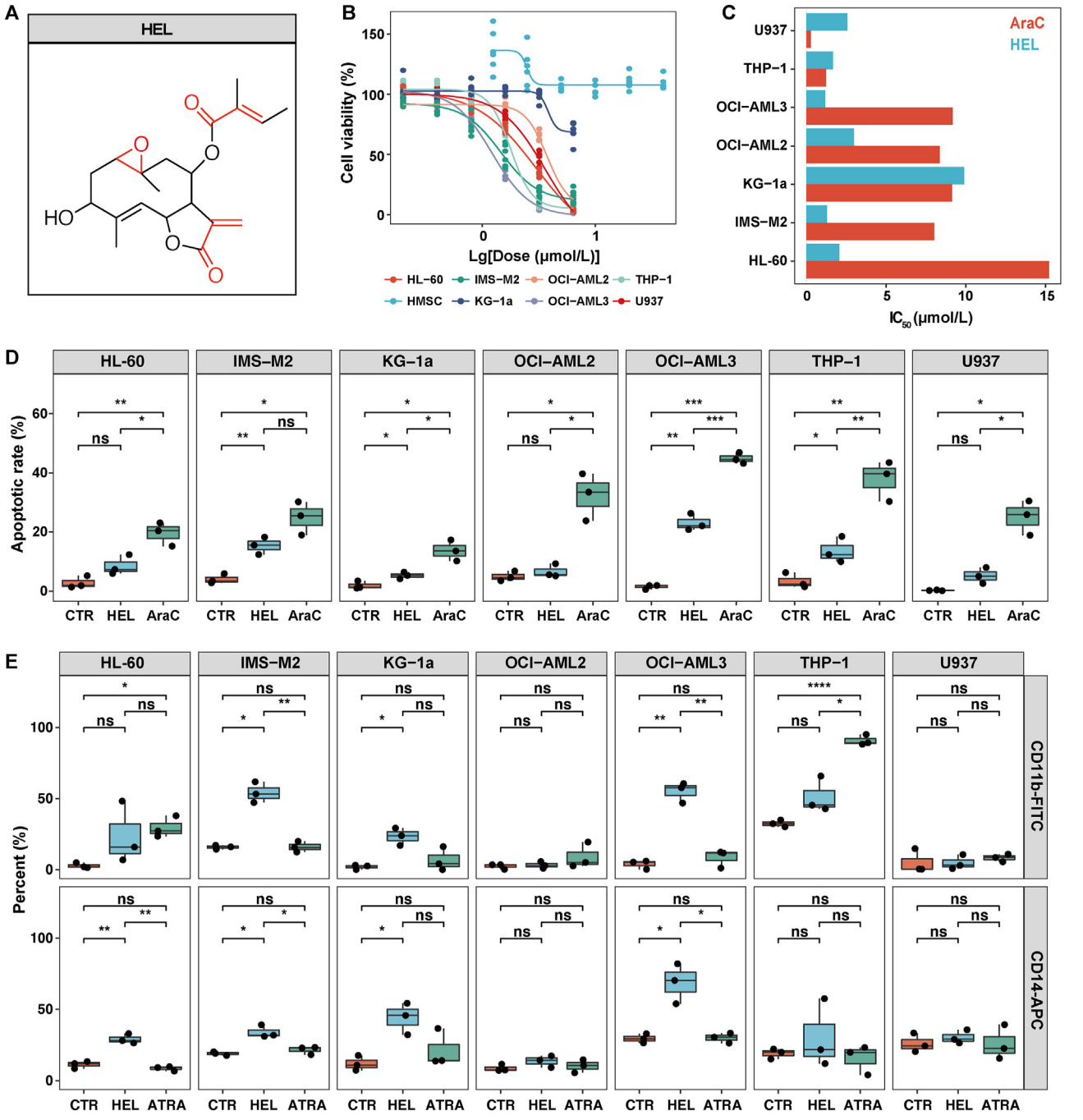

Figure 1 HEL inhibits cell proliferation, induces apoptosis and differentiation in AML cells. (A) Structure of HEL highlighting (in red) three potentially thiol reactive sites. (B, C) Calculation of IC_{50} for HEL using MTT dose response curves expressed as the log of concentration *vs.* cell viability of the AML or HMSC cells ($n = 5$). (D) the effect of HEL (5 μmol/L) on cell apoptosis of multiple AML cells was analyzed by FCM with AraC (5 μmol/L) as the positive group ($n = 3$). (E) AML cells were treated with DMSO, HEL (5 μmol/L) or ATRA (5 μmol/L) for 5 days as indicated. CD11b or CD14 expression was measured by FCM, the positive cell population percentage of CD11b or CD14 cells analysis results were presented ($n = 3$). Representative flow cytometry charts of experiments D and E are shown in Supporting Information Figs. S2 and S3, CTR means control group. All data are presented as Median ± IQR, ns, not significant, $^{*}P < 0.05$, $^{**}P < 0.01$, $^{***}P < 0.001$, $^{****}P < 0.001$.

with either vehicle (injection oil), 50 mg/kg HEL, or 50 mg/kg AraC by intraperitoneal injection every 48 h for 14 days. The mice were sacrificed at the end of the experiment. The bone marrow and spleen were dissected and tail vein blood was collected. The experimental details are shown in Fig. 3A.

For assessment of leukemia burden and differentiation, bone marrow was resuspended in ice-cold phosphate buffer extraction (PBE) (Supporting Information Table S1), filtered using a 40 μmol/L cell sieve, and washed twice with ice-cold PBE, then 1 mL red blood cell lysis buffer (#C3702, Beyotime, Jiangsu, China) was

added and centrifuged for 5 min at 1000 × *g*. Cells were then washed with ice-cold PBE twice and resuspended in 0.1 mL FCS buffer, blocked with 10 μL FcR blocking reagent (#16-0167-82; Miltenyi, North Rhine-Westphalia, Germany) for 10 min. Cells were washed and resuspended in 100 μL FCS buffer and stained with PE-anti-mouse CD45 (#12-0451-82, eBioscience) to analyze mouse leukocytes; PE-Cy5-anti-human CD45 (#15-0459-42, eBioscience) to analyze human leukocytes; and FITC-anti-human CD11b and APC-anti-human CD14 to analyze cell differentiation, according to the cell differentiation assay described in Section 2.5. Appropriate isotype controls were included in this experiment. Bone marrow cells were analyzed by FCM using the Gallios Flow Cytometer. FlowJo software was used to analyze the results.

The dissected spleens were weighed, paraffin-embedded, cut into 7-μm thick sections, and stained with hematoxylin and eosin. Images were obtained using an Axio Scope A1 microscope (Zeiss).

Blood samples were collected into a glass capillary tube. A complete blood count was performed using an automated hematology analyzer. Sample sizes were $n = 10$ mice for each treatment condition.

2.9. RNA-seq and data analysis

OCI-AML3 cells were incubated with either 5 μmol/L HEL or 0.1% DMSO in triplicate for 48 h. Total RNA was isolated using an RNeasy kit (#74004; Qiagen, Hilden, Germany). RNA libraries were prepared from 1 μg of total RNA using an mRNA-Seq Library Prep Kit (#001.24; Lexogen, Wien, Austria). Total RNA and library quality were analyzed using a Qubit 3.0 Fluorometer (Invitrogen, Carlsbad, CA, USA). Samples were sequenced using an Illumina HiSeq/Novaseq instrument according to the manufacturer's instructions (Illumina, San Diego, CA, USA). RNA-seq reads were aligned to the human genome using Hisat2 (v2.0.1) and gene expression was determined using HTSeq (v0.6.1). Differential expression was analyzed using the DESeq2 Bioconductor package (https://bioconductor.org/packages/release/bioc/html/DESeq2.html) with the parameters set to default. GOSeq (v1.34.1) was used to identify gene ontology (GO) terms from an annotated list of enriched genes with a significance of $P < 0.05$. Gene set enrichment analysis (GSEA) was performed using the Java GSEA Desktop Application with default parameters and the C5 ontology gene sets, which are provided as part of MSigDB V6.2 (https://www.gsea-msigdb.org/gsea/msigdb/index.jsp) as default screening gene sets.

2.10. Human clinical data analysis

Genomic data of samples from patients with AML were obtained from the open-source cancer genomics website cBioPortal by using the AML, OHSU, Nature 2018 Study (https://www.cbioportal.org/). This study included RNA-seq gene expression profiles of samples from patients with AML and their associated clinical data ($n = 450$ AML patients with RNA-seq data that included associated survival data, among which 102 patients carried the *NPM1* mutation). Individual sample expression profiles were scored against the C5 ontology gene sets at MSigDB 6.2 using GSEA.

Patients were stratified according to their correlation score with the preribosome, rRNA metabolic process, and ribosome biogenesis gene sets, and Kaplan−Meier survival analyses were conducted using the default settings in cBioPortal (https://www.cbioportal.org/). The log-rank test was used to assess statistical significance.

2.11. Northern blot analysis of pre-rRNA species

Northern blotting was conducted using a previously described method[30,31]. RNA (5 μg/well for cytoplasmic extracts) was separated on a 1% agarose gel with 1 × TT buffer (30 mmol/L triethanolamine and 30 mmol/L tricine, pH 7.9) containing 1% formaldehyde and run in 1 × TT buffer at 120 V. RNA was transferred to an N^+ nylon membrane (#FFN10; Beyotime) and fixed by UV cross-linking. Membranes were prehybridized for 2 h at 48 °C in 6 × SSC buffer (#T9172, TaKaRa, Shiga, Japan), 5 × Denhardt's solution (#750018, Invitrogen), 0.5% SDS, 50% formamide (#75-12-7, Macklin), and 100 μg/mL denatured herring sperm DNA (#B548210-0005, Sangon Biotech, Shanghai, China). Biotin-labeled oligodeoxynucleotide probe was added and incubated overnight at 48 °C. The 3′-biotin-labeled ITS1, ITS2, and ETS probes used in this study were provided by Sangon Biotech Co., Ltd. and their sequences were as follows:

ETS (5′−3′): TCGGACGCGCGAGAGAACAGCAGG;
ITS1 (5′−3′): CCTCGCCCTCCGGGCTCCGGGCTCCGTTAATGATC;
ITS2 (5′−3′): CTGCGAGGGAACCCCCAGCCGCGCA.

After hybridization, the membranes were washed in 2 × SSC for 10 min at room temperature and then in 1 × SSC for 10 min at room temperature. Labeled RNA signals were detected using the Chemiluminescent Biotin-labeled Nucleic Acid Detection Kit (#D3308, Beyotime), images were captured using the Tanon 5200 Chemiluminescent Imaging System, and the captured signal was quantified using ImageJ 1.52 (National Institutes of Health, Bethesda, MD, USA).

2.12. Immunofluorescence (IF)

Mouse anti-human fibrillarin (FBL, #16201-1-AP) and rabbit anti-human NPM1 (#60096-1-Ig) primary antibodies, and corallite 594 goat anti-rabbit IgG (#SA0003-4) and corallite 488 goat anti-mouse IgG (#SA0003-1) secondary antibodies were purchased from Proteintech (Wuhan, China). Cells were fixed on coverslips for 15 min with 4% paraformaldehyde in PBS, rinsed three times with PBS, and permeabilized with 0.2% Triton X-100 (#ST795, Beyotime) for 20 min. After rinsing three times, the cells were incubated with 1% bovine serum albumin (BSA) in PBST (#28352; ThermoFisher Scientific, Waltham, MA, USA) for 30 min, then with the primary antibody in the same buffer at 4 °C overnight. The dilution factor used for primary antibodies was 1:200. The cells were washed three times in PBST, and nonspecific sites were further saturated with 1% BSA in PBST for 30 min. Cells were then incubated for 1 h with the corresponding secondary antibodies (1: 500 dilution). After rinsing twice with Hoechst 33342 (#ab228550; Abcam, Cambridge, UK), the coverslips were mounted and analyzed using a Leica TCS SP8 confocal microscope (Leica, Wetzlar, Germany).

2.13. QTRP assays

QTRP studies were performed following a previously reported method[28]. Briefly, OCI-AML3 cells were treated with DMSO or the indicated concentrations of HEL for 48 h. Cells were then harvested and lysed by probe sonication in protein lysis buffer (Table S1), and protein concentrations were determined using a BCA protein assay kit (#ab102536, Abcam). Proteins (2.5 mg)

were then labeled with 100 μmol/L IPM (#EVU111; Kerafast, Boston, MA, USA) at room temperature for 1 h, following reduction with DTT (#125B0424; YIFEIXUE Biotech, Nanjing, China) and alkylation with iodoacetamide (#DI8451, Bomeibio), as described previously. The protein was then precipitated using the methanol−chloroform method. Protein samples were processed into tryptic peptides using trypsin digestion buffer (Table S1) containing 1 mol/L urea. After desalting using HLB SPE cartridges (#161A38289A; Waters Corp., Milford, MA, USA), the IPM probe-modified peptides were tagged with isotopically labeled azido-biotin reagents containing a photo-cleavable linker (#EVU102, # EVU151, Kerafast) *via* copper-catalyzed azide-alkyne cycloaddition (CuAAC). After CuAAC, proteins were washed and combined in a 1:1 vehicle:HEL ratio, washed again, and bound to streptavidin-agarose beads (#20347, ThermoFisher Scientific) while rotating for 2 h at room temperature in streptavidin binding buffer (Table S1). After washing the beads with washing buffer (Table S1), the beads were exposed to 365 nm UV light for 2 h at room temperature. After centrifuging at 2000 × *g* for 4 min, the supernatant was concentrated and desalted using C18 stage tips (#87782, ThermoFisher Scientific) and HLB SPE cartridges, respectively, according to the literature[28]. The photo-released peptides were subsequently identified and quantified by mass spectrometry-based shotgun proteomics using a Q-Exactive Plus Qrbitrap (ThermoFisher Scientific). Finally, the MS data were interpreted by a streamlined informatic pipeline using the pFind 3 (https://github.com/pFindStudio/pFind3) software and an automatic post-processing algorithm.

2.14. *RPS2 WT and C222S mutant protein expression and purification*

A pET28 vector containing full-length human RPS2 with a His-tag was provided by the Public Protein/Plasmid Library (PPL, Nanjing, China). The RPS2-C222S plasmid was prepared using the QuickMutation Plus Site-Directed Mutagenesis Kit (#D0208S, Beyotime) using the pET28-His-RPS2 plasmid as a template. The primers were provided by Sangon Biotech Co., Ltd., and had the following sequences: forward, 5′-GGGCTGAGGTGTAGCTGTCATCGATACCAGC-3′; reverse, 5′-GCTGGTATCGATGACAGCTACACCTCAGCCC-3′. All plasmids were overexpressed in *Escherichia coli* BL21(BE3) cells in LB medium (#ST158; Beyotime) in the presence of 50 mg/mL kanamycin (#R31000, Yuanye Biotech, Shanghai, China). Cells were grown at 37 °C to an optical density of 0.8 and induced with 0.5 mmol/L IPTG (#ST098, Beyotime) for 4 h at 25 °C. Samples were collected by centrifugation. Cell pellets were sonicated in lysis buffer (Table S1) and the lysate was centrifuged at 5000 × *g* for 10 min. His-Tag Purification Resin (#P2233, Beyotime) was mixed with the lysate supernatant for 1.5 h and washed with lysis buffer. The beads were then transferred to a column, and the bound protein was washed with 15% washing buffer and then eluted with 100% washing buffer (Table S1). The proteins were enriched by ultrafiltration using ultrafiltration spin columns (15 mL, 10 kDa MWCO, PES; Sartorius, Göttingen, Germany) and preserved in PBS containing 20% glycerol at −80 °C.

2.15. *Gel-based ABPP*

As described previously[26,32], recombinant proteins including WT and C222S RPS2 mutant (0.3 μg per sample) were pretreated with either DMSO or indicated concentrations of HEL at 37 °C for 1 h in 20 μL PBST (#P0226, Beyotime), and subsequently treated with 500 nM IA-rhodamine (#114458-99-0, J&K Scientific, Beijing, China) at room temperature for 1 h. The reaction was stopped by the addition of 4 × SDS protein loading buffer (#WB2001; New Cell & Molecular Biotech Co., Ltd.). After boiling at 95 °C for 5 min, the samples were separated using SDS-PAGE. IA-rhodamine probe-labeled proteins were analyzed using a GelDoc XR (Bio-Rad, Hercules, CA, USA).

2.16. *Microscale thermophoresis (MST) assay*

As described previously[33], the equilibrium dissociation constant (K_D) was determined using a Monolith NT.115 instrument (NanoTemper Technologies, San Francisco, CA, USA). His-tagged RPS2 WT or C222S mutant proteins were fluorescently labeled using the His-Tag Labeling Kit (#MO-L018, NanoTemper Technologies) according to the manufacturer's protocol. HEL was diluted to the indicated concentrations and incubated with either WT or C222S mutant proteins (0.5 mg/mL) for 15 min. The samples were then loaded into glass capillaries. The K_D values were calculated from triplicate measurements using the mass action equation *via* the NanoTemper software.

2.17. *MS-based co-immunoprecipitation*

Co-immunoprecipitation (Co-IP) with MS sample preparation was performed as previously described[34,35]. Briefly, the OCI-AML3 cells were washed twice with PBS and pelletized. The cross-linking reaction was performed using 2 mmol/L disuccinimidyl sulfoxide (DSSO) (#A33545, ThermoFisher Scientific) in 1 mL PBS for 1 h. The reaction was quenched with 50 mmol/L Tris−HCl (pH8.0) (#ST780, Beyotime), and cells were lysed in Co-IP lysis buffer (#P0013, Beyotime). The lysate was pelleted at 12,000 × *g* for 20 min at 4 °C. The protein concentration of the cytosolic fraction was adjusted to 500 μg after the BCA assay. Thirty microliters of protein AG beads (#P2108, Beyotime) were equilibrated with 1 mL wash buffer (#ST661, Beyotime) and incubated with 500 μg protein lysate and approximately 5 μg RPS2 (#ab154972, Abcam) or MDM2 (#66511-1-Ig, Proteintech) antibody or a corresponding amount of rabbit IgG isotype control (#14-4616-82, eBioscience) overnight at 4 °C. The beads were washed twice with wash buffer and twice with basic buffer (Table S1). For the MS sample, 25 μL elution buffer 1 (Table S1) was added to the beads for 30 min at room temperature. Subsequently, the beads were treated with 100 μL elution buffer 2 (Table S1) overnight at 37 °C. Protein digestion was stopped with 0.75% trifluoroacetic acid, and peptides were concentrated with a centrifugal vacuum concentrator and desalted using C18 stage tips (#87782, ThermoFisher Scientific) according to previously published methods. Peptides were subsequently identified and quantified by mass spectrometry-based label-free proteomics using a Q-Exactive Plus Qrbitrap (ThermoFisher Scientific). Finally, the MS data were processed using MaxQuant software (version 1.6.0.1), and the resulting data were statistically analyzed using Perseus software (version 1.6.2.3) according to previously described methods[33,34].

2.18. *Constructing knockdown lines and reinforced expression and overexpression*

Short hairpin (*sh*) oligonucleotides were used to knockdown *p53* expression in OCI-AML3 cells. Lentiviral plasmids containing

*sh*p53 (PPL) were transfected into 293T cells using Lipofectamine 6000 (#C5026, Beyotime). Lentivirus was collected from the filtered culture medium and used to infect the target cell line with a 1:1000 dilution of polybrene. OCI-AML3 cells were selected over 3 d with 1 μg/mL of puromycin (#ST551, Beyotime). The short hairpin sequences used for the generation of the knockdown cell line are provided in the Supporting Information Table S2.

OCI-AML3 cells were transiently transfected with an *RPS2* expression plasmid using Lipofectamine 6000 for the expression of WT or C222S mutant *RPS2*. The WT human *RPS2* expression plasmid contained a C-terminal FLAG tag and was purchased from PPL. The C222S *RPS2* mutant was generated using a QuickChange site-directed mutagenesis kit, according to the manufacturer's instructions.

For transient knockdown of *RPS2* or *NPM1* with small interfering RNA (siRNA), cells were seeded in 6-well plates overnight and then transfected with either non-targeting siRNA oligonucleotides (si*NC*, Sangon Biotech) or si*RPS2* (or si*NPM1*) oligonucleotides (Sangon Biotech, for sequences see Table S2) using Lipofectamine 6000. Cells were treated with DMSO or HEL 48 h after transfection to determine the *in vitro* protein expression.

2.19. Co-IP pulldown assays

For FLAG pulldown assays, OCI-AML3 cells stably expressing FLAG-GFP, FLAG-RPS2, or FLAG-RPS2 (C222S) were treated with DMSO or 5 μmol/L HEL for 48 h. Cells were collected, washed with ice-cold PBS, and lysed by probe sonication in Co-IP lysis buffer (#P0013, Beyotime). After centrifugation at 12,000 × *g* for 10 min at 4 °C, the supernatant was incubated with BeyoMag Anti-Flag Magnetic Beads (#P2115, Beyotime), washed twice with cold TBS (#ST661, Beyotime), and the beads were added to SDS-PAGE sample loading buffer (#P0015, Beyotime) and boiled at 95 °C for 5 min. The supernatants were used for Western blot analyses.

For MDM2 pulldown assays, OCI-AML3 cells were treated with DMSO or 5 μmol/L HEL for 24 h, washed with cold PBS, and lysed with Co-IP lysis buffer. MDM2 was precipitated using protein A/G magnetic beads according to the manufacturer's instructions; PBS was used for the washes. A specific isotype control antibody served as the control. The amounts of *MDM2*, *p53*, and *RPL11* in the pulldown fractions were analyzed by Western blot analysis.

For statistical analyses, the results of each biological replicate were set to a 1.0-fold ratio.

2.20. Western blot

RPS2 antibody was obtained from Abcam (#ab155961). Antibodies against p53 (#EA780B), caspase 3 (#E1A0835B), beta-tublin (#E301044), histone-H3(#E1A0435B-3), and cleaved caspase 3 (#EA003L) were obtained from Enogene Biotech (Nanjing, Jiangsu, China). Antibodies against p21 (#2947S) and GAPDH (#5174S) were obtained from Cell Signaling Technology (Danvers, MA, USA). Antibodies against c-MYC (#1028-1-AP), CEBP/α (#18311-1-AP), RPL11 (#16277-1-AP), MDM2 (#66511-1-Ig), FLAG (#66008-4-Ig), β-actin (#20536-1-AP) and NPM1 (#60096-1-Ig) were purchased from Proteintech (Wuhan, Hubei, China).

Proteins were resolved by SDS-PAGE and transferred to PVDF membranes. Membranes were blocked with 5% BSA in PBS-T solution for 2 h at room temperature, washed with PBS-T, and probed with primary antibodies diluted in the recommended diluent overnight at 4 °C. After three washes with PBS-T, the membranes were incubated with the indicated secondary antibodies at a 1:5000 dilution in 5% BSA in PBS-T at room temperature for 2 h. Membranes were washed in PBS-T five times, and signals were detected using the Super ECL Detection Reagent Kit (#36208ES800, Yeasen Biotechnologies) according to the manufacturer's protocols. Images were captured by the Tanon 5200 Chemiluminescent Imaging System (Tanon, Shanghai, China), and the signal intensity was quantified using ImageJ 1.52 (NIH).

2.21. Quantitative RT-PCR

Total RNA was extracted using Trizol reagent (#15596018, Invitrogen) follow by reverse transcription using RevertAid First Strand cDNA Synthesis kit (#K1622, Thermo). Gene-specific primers and SYBR Green qPCR Mix kit (#D7265, BeyoFast) were used to quantify mRNA levels of indicated genes. The real time PCR reactions were performed in triplicate on ABI7500 (Thermo). The primer sequences used are listed in Table S2.

2.22. Statistical analysis

All the statistical tests were performed with RStudio (USA) open-source software (V1.3.959) using the "ggpubr" package (V 0.4.0). Two-tailed Student's *t* test or one-way analysis of variance (ANOVA) were applied to determine statistical significance. All data presented as median ± interquartile range (IQR), significance was described as follows: ns, not significant, $^{*}P < 0.05$, $^{**}P < 0.01$, $^{***}P < 0.001$, $^{****}P < 0.0001$.

3. Results

3.1. In vitro activity showed that HEL selectively inhibits the proliferation of NPM1 mutant AML cells, promotes cell differentiation, induces apoptosis, and arrests cell cycle

We first evaluated the effect of HEL (chemical structure see Fig. 1A) on the proliferation of different AML cells, as shown in Fig. 1B and C and Supporting Information Table S3. HEL inhibited the proliferation of seven AML cell lines, including U937, THP-1, OCI-AML3, IMS-M2, OCI-AML2, KG1a, and HL60, at concentrations ranging from 0.2 to 12.8 μmol/L. Among these cell lines, the *NPM1* mutant AML cell line OCI-AML3 and IMS-M2 were the most sensitive to HEL, with an IC_{50} of 1.17 and 1.28 μmol/L, respectively, which was more sensitive than AraC, which is an approved clinical chemotherapy drug[1,2]. A toxicity evaluation showed that HEL did not inhibit the proliferation of normal bone marrow mesenchymal stem cells (HMSC) in the concentration range of 1.25−40 μmol/L, while AraC was significantly more toxic with an IC_{50} of 25.2 μmol/L (Table S3).

The results of apoptosis assay showed that HEL significantly induced apoptosis in four AML cell lines including IMS-M2, OCI-AML3, KG-1a, and THP-1, at a dosing concentration of 5 μmol/L (Fig. 1D and Supporting Information Fig. S2). The strongest apoptosis induction was observed in *NPM1* mutant AML cells OCI-AML3, IMS-M2 with apoptosis rates of 23.07 ± 2.87% and 15.93 ± 2.94%, respectively.

We then evaluated the effect of HEL on the differentiation of each AML cell line by evaluating differences in the expression levels of CD11b (granulocytes) and CD14 (monocytes) on the membrane of each cell before and after drug administration using

flow cytometry. As shown in Fig. 1E and Supporting Information Fig. S3, at a concentration of 5 μmol/L, HEL significantly promoted the differentiation of OCI-AML3 ($P = 0.0023$), IMS-M2 ($P = 0.01$) and KG-1a ($P = 0.02$) cells to the granulocyte lineage and of OCI-AML3 ($P = 0.035$), IMS-M2 ($P = 0.02$) and HL-60 ($P = 0.026$) cells to the monocyte lineage after five days of administration compared to the control group, whereas the current clinical pro-differentiation drug ATRA[36] only promote differentiation of acute promyelocytic leukaemia (APL) cell line HL-60 and the acute monocytic leukaemia cell line THP-1 to the granulocyte lineage. The above results suggest that, in addition to inhibiting proliferation and inducing cell apoptosis, HEL can significantly promote some AML cells, particularly *NPM1* mutant AML cells, to differentiate into monocytic and granulocytic lineages when administered at the appropriate time.

It was previously reported that expression levels of the transcription factor *p53* decreased in *NPM1* mutant AML cells due to the abnormal localization of NPM1c protein in the cytoplasm[8,9]. In this experiment, we found that the expression of p53 protein in NPM1 mutant AML cell lines, including OCI-AML3 and IMS-M2 was significantly up-regulated ($P < 0.01$) after the administration of HEL at 5 μmol/L, while this effect was not significant in other AML cell lines (Supporting Information Fig. S4). Above results suggest that the sensitivity of HEL to *NPM1* mutant AML may be related to its specificity in increasing the expression of p53 protein in these cells.

Subsequently, the activity of HEL against its most sensitive cell line OCI-AML3 was further evaluated *in vitro*. As shown in Fig. 2A, an apoptosis assay showed that HEL significantly induced apoptosis in OCI-AML3 cells at concentrations of 5−10 μmol/L in a dose-dependent manner. Cells showed significant monocytic morphological changes at a HEL concentration of 5 μmol/L, verifying the previous results of the differentiation assay (Fig. 2B, blue and purple arrows). As shown in Fig. 2C, detection of CD11b and CD14, markers of cell differentiation, by flow cytometry showed that OCI-AML3 cells differentiated into monocytic and granular lineages at HEL concentrations of 5 and 10 μmol/L, respectively, and that the level of differentiation was dose-dependent. The expressions of granulocyte colony-stimulating factor receptor (*CSF3R*) and macrophage colony-stimulating factor receptor (*CSF1R*) were upregulated more than 5 or 15-folds when OCI-AML3 cells treated with 5 μmol/L of HEL (Fig. 2D), further prove the ability of this compound to induce cell differentiation in *NPM1*-mutated AML cells. Cell cycle assays in OCI-AML3 cells also showed (Fig. 2E) that HEL significantly arrested the cell cycle in the G1/S phase at concentrations of 5 and 10 μmol/L in a dose-dependent manner. Western blotting showed that HEL significantly increased the expression levels of p53 and decreased c-MYC expression levels in OCI-AML3 cells in a dose-dependent manner. At the same time, the expression level of the *p53*-regulated apoptosis-related protein c-Cas3 increased significantly as the dose of HEL increased, and the expression level of cyclin p21 (regulated *via* the p53−p21 axis)[37], which controls the cell cycle during the G1 phase, and CEBP/α (regulated *via* the p53−KLF4−CEBP/α axis)[38], which related to cell differentiation of AML, increased significantly with increasing doses of HEL, which is consistent with the results of flow cytometry (Fig. 2F and Supporting Information Fig. S5).

In summary, *in vitro* results demonstrate that *NPM1* mutant AML cells were the most sensitive to HEL *in vitro*, resulting in significant inhibition of proliferation, induction of apoptosis, cell cycle arrest in the G1 phase, and granular and monocytes differentiation in AML cells without significant toxicity to normal mesenchymal stem cells. Some of these functions are superior to those of AraC, the drug of choice for clinical chemotherapy, and unlike the pro-differentiation drug ATRA, HEL promotes the differentiation of *NPM1* mutant AML cells.

3.2. *In vivo activity showed that HEL significantly inhibited proliferation and promoted the differentiation of NPM1 mutant AML cells in the bone marrow of M-NSG mice*

As shown in Fig. 3A and B and Supporting Information Fig. S6, following two weeks of treating OCI-AML3 cells (human $CD45^+$ cells) with HEL at a dose of 50 mg/kg every other day, proliferation was significantly decreased in the bone marrow of M-NSG mice compared to that in the model group ($P < 0.0001$). In addition, no significant difference was observed in proliferation when compared to the positive control drug AraC at the same dose, suggesting that AraC has inhibitory activity against *NPM1* mutant AML cells *in vivo*.

As shown in Fig. 3C, flow cytometry results showed that HEL significantly increased the expression levels of CD11b and CD14 ($P < 0.0001$ and $P = 0.00031$, respectively) in the bone marrow of M-NSG mice compared with those in the model group, whereas AraC applied at the corresponding dose did not have this effect. This suggests that, consistent with the *in vitro* results, HEL can promote the differentiation of *NPM1* mutant AML cells to granulosa and monocytic lineages *in vivo*.

We also found that HEL administration significantly reduced spleen weight ($P = 0.015$) and the level of splenic lesions of model mice (Fig. 3D and E). Peripheral blood data suggest that HEL significantly reduced the number of white blood cells ($P = 0.024$) and significantly increased the number of platelets ($P = 0.001$) in model mice (Fig. 3F).

In conclusion, HEL significantly inhibited the proliferation of *NPM1* mutant AML cells in the bone marrow *in vivo*, promoted their differentiation into granular and monocytic lineages, and reduced the infiltration of malignant AML cells in the spleen of model mice, while reducing the number of white blood cells and elevating platelets. It also reduced the level of splenic lesions of AML model mice.

3.3. *HEL disrupts the processing of ribosomal RNA, causing nucleolar stress in NPM1 mutant AML cells*

RNA-Seq was used to screen for pathways targeted by HEL in OCI-AML3 cells. As shown in Supporting Information Figs. S7A, 6694 differentially expressed genes were identified after HEL treatment, of which 3671 genes were downregulated and 3023 were upregulated. These genes were subjected to GO pathway enrichment analysis (Fig. S7B), and we found that HEL significantly inhibited the ribosome biogenesis (Log$P = 31.75$) and rRNA processing (Log$P = 7.77$) pathways in *NPM1* mutant AML cells.

Next, by analyzing the GSEA of the transcriptomics database of AML clinical patients published in *Nature* in 2018 (https://github.com/cBioPortal/datahub/issues/402), we found that the rRNA metabolic process pathway (normalized enrichment score [NES] = 1.80, $P < 0.01$), preribosome pathway (NES = 1.74, $P < 0.01$), and ribosomal biogenesis pathway (NES = 1.80, $P < 0.01$) were significantly upregulated in *NPM1* mutant AML patients ($n = 100$) as compared to patients with the wild-type gene ($n = 267$). GSEA of the transcriptome data for HEL-treated OCI-AML3 cells indicated that all three ribosomal pathways

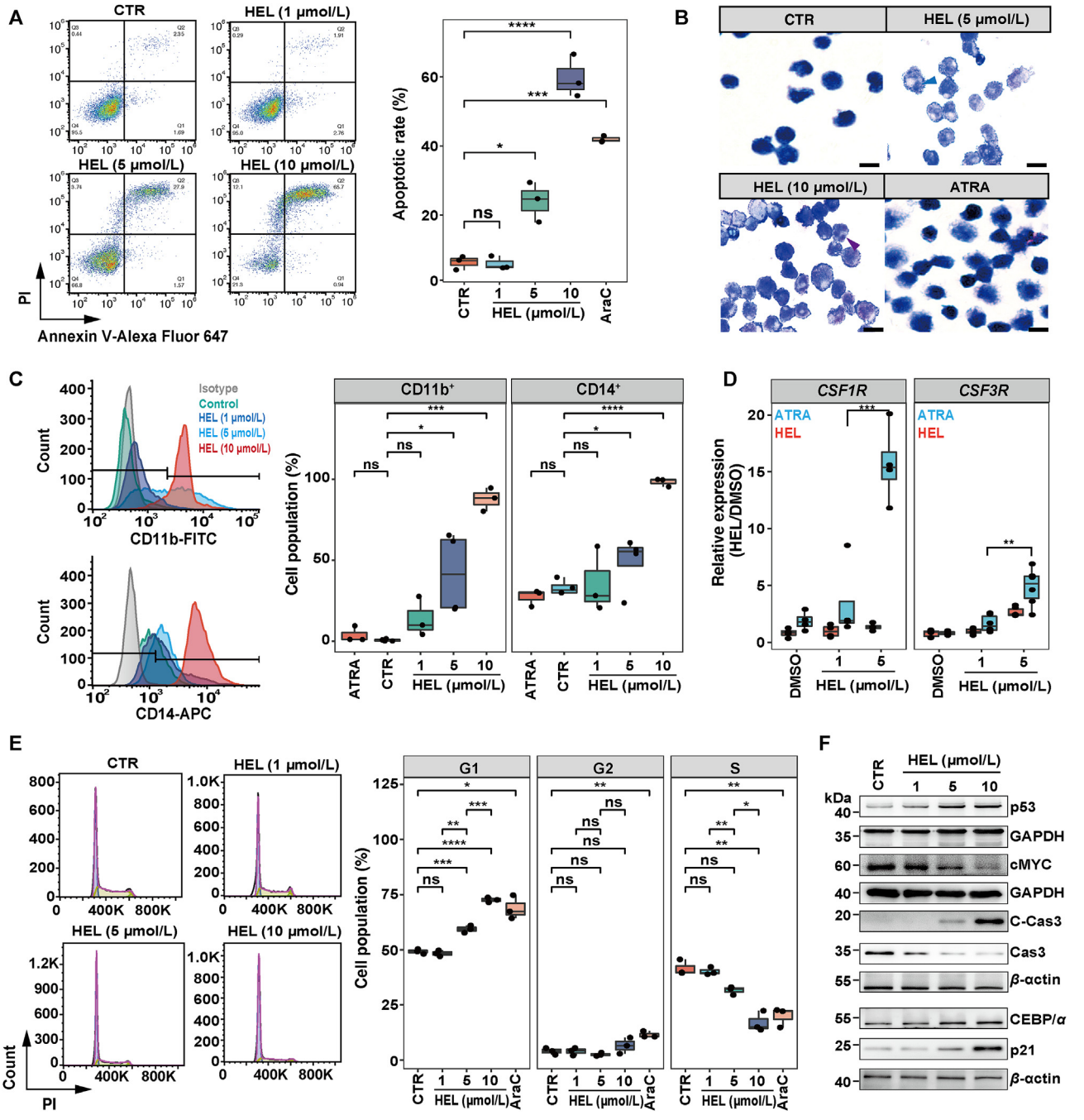

Figure 2 HEL induces apoptosis, cell cycle arrest and cell differentiation of *NPM1*-mutated AML cells in dose dependent manner. (A) the effect of HEL on cell apoptosis of OCI-AML3 cells was analyzed by FCM with AraC (5 μmol/L) as the positive group. (B) Cell morphology of OCI-AML3 after HEL or ATRA (positive group) treatment on Day 5. Giemsa-stain, scale bar, 50 μm. (C) The effect of HEL on cell differentiation of OCI-AML3 cells was analyzed by FCM, right panel shows the percentage of $CD11b^+$ or $CD14^+$ cells after HEL treatment at different doses. (D) Macrophage colony stimulating factor receptor (*CSF1R*) or granulocyte colony stimulating factor receptor (*CSF3R*) expression analyzed by RT-qPCR in OCI-AML3 cells after 5 days of HEL treatment. (E) HEL induces a dose-dependent cell cycle arrest at G1 phase in OCI-AML3 cells. AraC (5 μmol/L) was used as the positive group. All the above experiments were analyzed by three biological replicates, presented as Median ± IQR, ns, not significant, $*P < 0.05$, $**P < 0.01$, $***P < 0.001$, $****P < 0.0001$. (F) Protein levels of p53, cMYC, C-Cas3, Cas3, CEBP/α and p21 in OCI-AML3 cells were analyzed by Western blot after HEL treatment at different doses ($n = 3$). The expressions are quantified in Supporting Information Fig. S5.

mentioned above were significantly downregulated, with NES values of −2.58, −2.50, and −2.65, respectively (Fig. 4A and B, and Fig. S7C).

In addition, using the same clinical patient database, we found that the rRNA metabolic process and proteasome pathway had a significant impact on the survival and prognosis of AML patients.

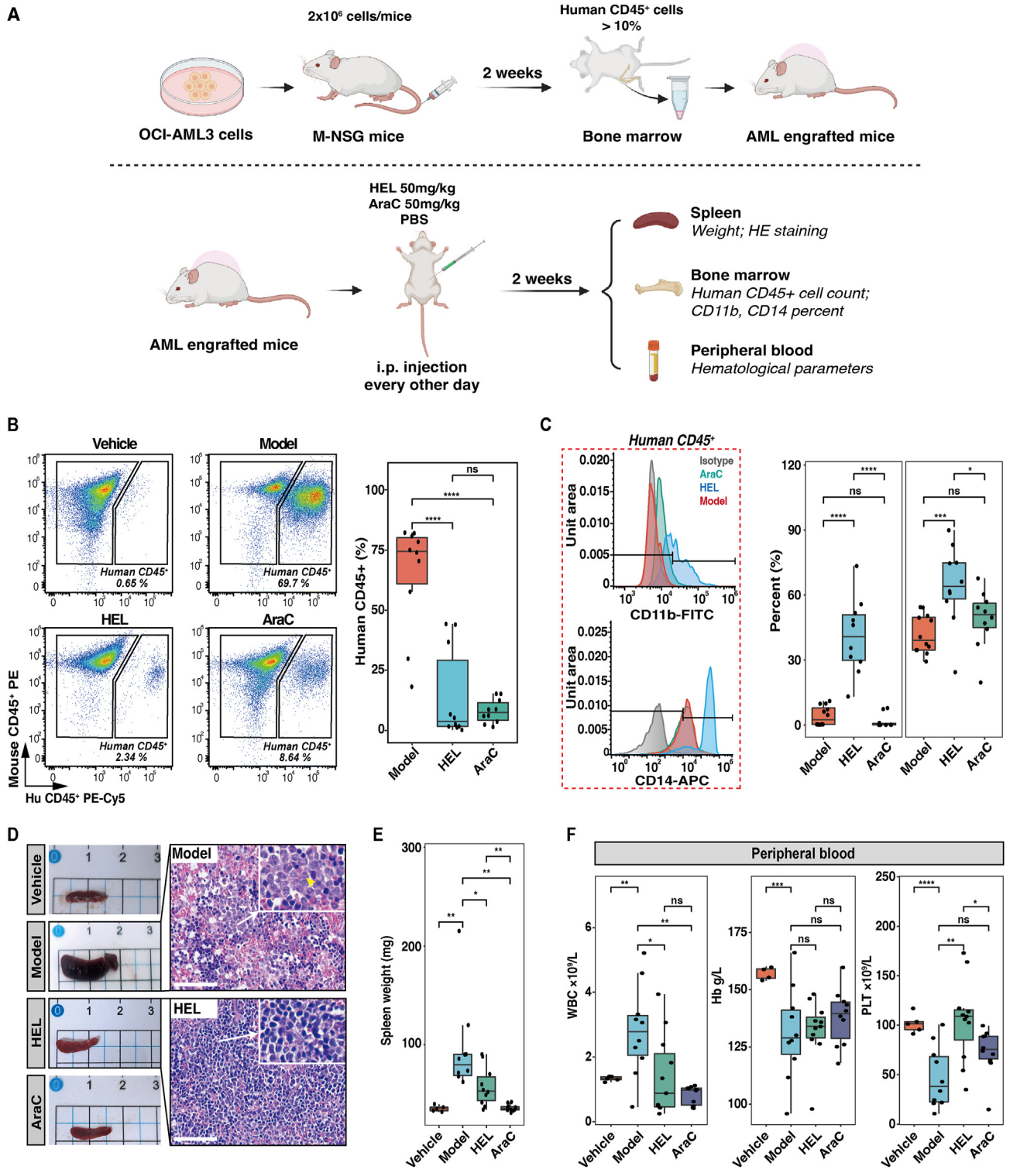

Figure 3 The *in vivo* effect of HEL on NPM1 mutant AML cells. (A) Experiment schema. After confirmation of bone marrow AML engraftment to >10% in 3 randomly selected mice, remaining mice were randomized to model, 50 mg/kg HEL, or 50 mg/kg AraC, by i. p. every 48 h for 14 days (B) Bone marrow AML burden. Representative flow cytometry for Human $CD45^+$ (AML) and mouse $CD45^+$ (normal) cells. (C) Granulocyte (CD11b) and monocyte (CD14) lineage differentiation marker expression in marrow AML cells using FCM analysis. (D, E) Photos show spleens from model M-NSG mice and different treatment groups, with H&E-stained spleen sections showing splenic lesions (yellow arrow). Scale bar, 12 μm. (F) Serial blood counts. The increasing of WBC and decreasing of Hb or PLT was due to myeloblasts. All the above experiments were analyzed by ten mice per group (vehicle group, $n = 5$), presented as Median ± IQR, ns, not significant, $^*P < 0.05$, $^{**}P < 0.01$, $^{***}P < 0.001$, $^{****}P < 0.0001$.

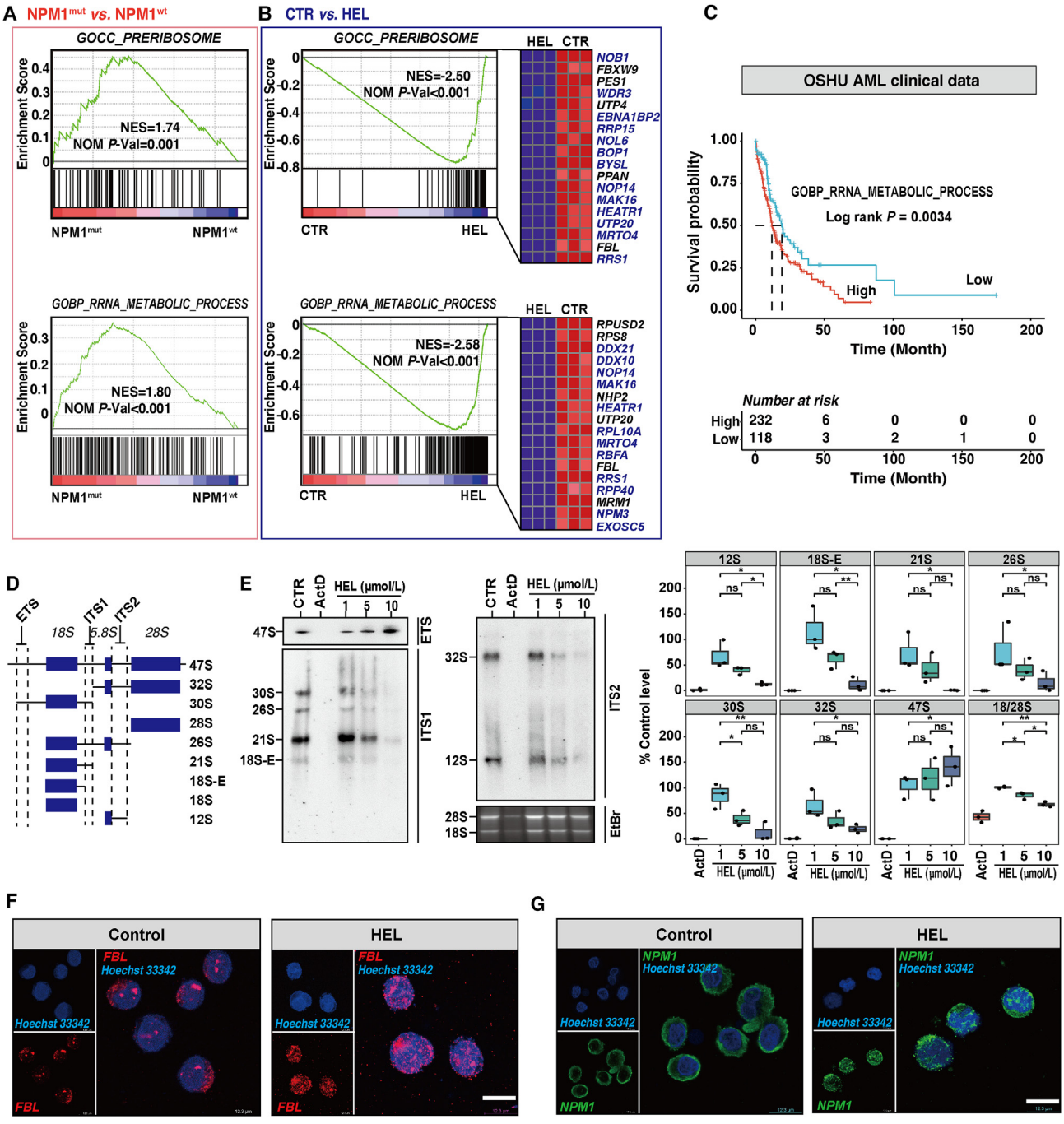

Figure 4 HEL regulates ribosome RNA metabolic process and causes nucleolar stress in *NPM1* mutant AML cells. (A, B) GSEA enrichment plots of preribosome or rRNA metabolic process genesets in *NPM1* mutant AML patients group compared with WT (red) or OCI-AML3 cells treated with DMSO compared with HEL (blue). Heat map of the preribosome or rRNA metabolic process genesets containing top 20 genes found significantly down-regulated when comparing DMSO treated OCI-AML3 cells *versus* the HEL treated. Genes in blue were found up-regulated in the *NPM1* mutant patients against WT ones. (C) Kaplan−Meier plots shows that high expression of rRNA metabolic process gene-set was associated with shorter overall survival time in AML patients significantly. (D, E) Northern blot analysis of pre-rRNA processing phenotypes after the treatment of HEL at different concentrations in OCI-AML3 cells, ActD was set as positive group. The probes used in the screening (ETS, ITS1, and ITS2), as well as the major pre-rRNA detected, are depicted in the left. Mature rRNAs were shown on the ethidium bromide (EtBr)-stained gel. Bands on the Northern blots or EB gels ($n = 3$) were quantitated by ImageJ, presented as Median ± IQR, ns, not significant, $^*P < 0.05$, $^{**}P < 0.01$. (F, G) FBL (red) and NPM1 (green) localization in the HEL treated OCI-AML3 cells by IF. Hoechst 33342 (blue) was used to stain for nuclei. Images by Leica SP8 confocal microscope. Scale bar, 12.3 μm. Quantification of percentage of cells with nucleolar stress is shown in Supporting Information Fig. S8.

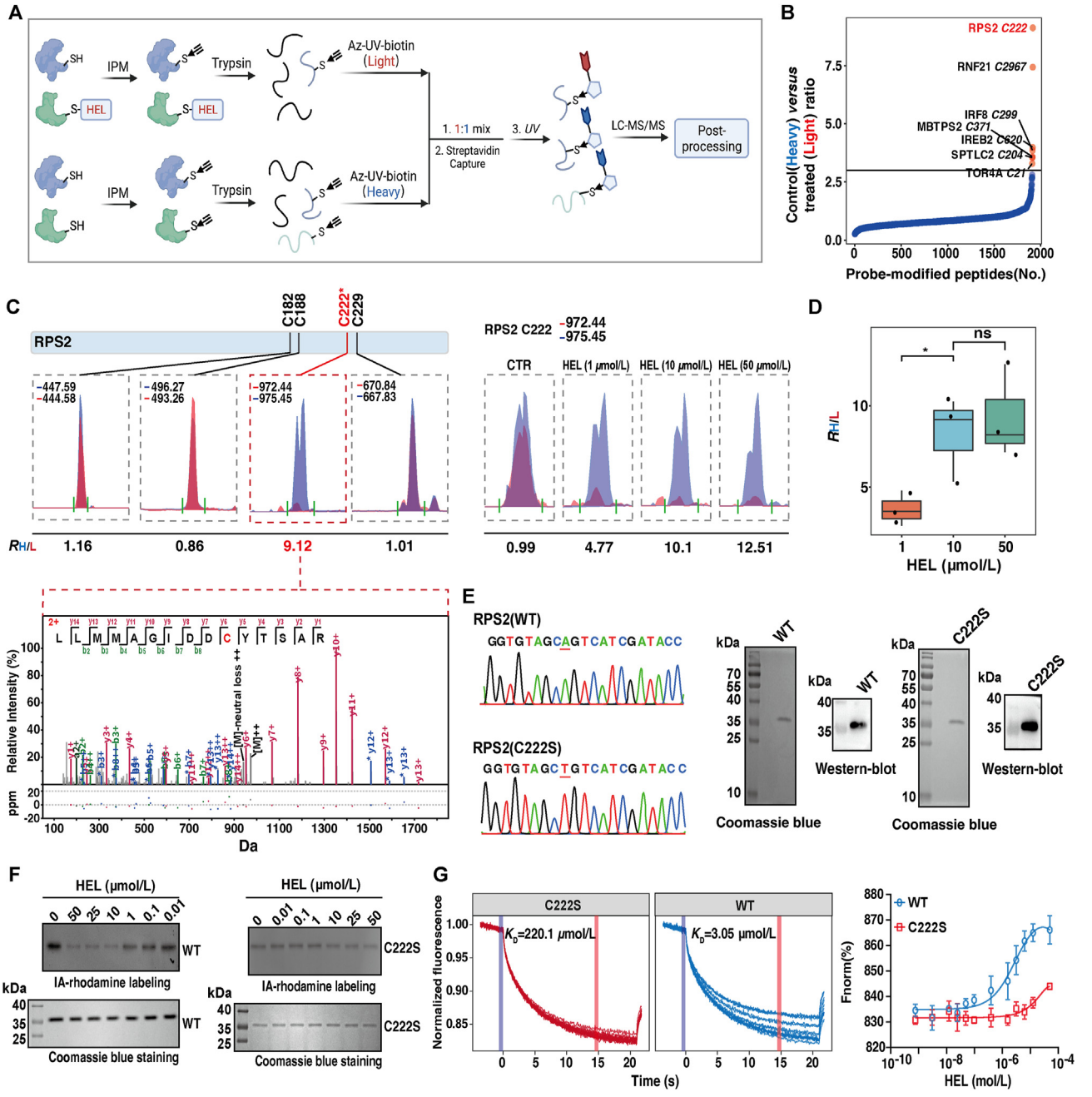

Figure 5 HEL targets C222 of RPS2 in *NPM1* mutant AML cells. (A) General protocol for QTRP. The proteome from HEL or DMSO (control) treatment with OCI-AML3 cells are labeled with IPM probe *in vitro* and then digested by trypsin, the peptides were conjugated with Light (L) and Heavy (H) Az-UV-biotin reagents, respectively, mixed and captured with streptavidin beads. The probe modified peptides are photo-released for further LC−MS/MS analysis, followed by pFind3 software analysis and post-processing. (B) Distribution of competitive QTRP ratios ($R_{H/L}$ values) quantified from reactions with the human OCI-AML3 proteome treated with 10 μmol/L HEL (three technical replicates from three biological replicates). A cutoff of threefold or greater blockade of IPM probe labeling ($R_{H/L} > 3$) is shown by black line to mark cysteines that exhibit high sensitivity to HEL, and proteins with cysteines showing the strongest competitive reactivity with HEL are labeled by names. (C) Left: representative MS1 profiles for multiple cysteine-containing peptides from the RPS2 protein, only the peptide containing C222 (MS2 profile underneath) shows sensitivity to HEL competition. Right: representative MS1 profiles for HEL-sensitive C222 peptide in RPS2 showing concentration-dependent blockade of IPM labeling by HEL. (D) Box plots showing the $R_{H/L}$ values C222 peptide of RPS2 quantified from competitive QTRP experiments with the OCI-AML3 proteome treated with 1, 10 and 50 μmol/L HEL, respectively, data were shown in three biological replicates. Data are presented as Median ± IQR, ns, not significant, $*P < 0.05$. (E) Left: Successful plasmid mutagenesis was verified by Sanger sequencing. Mutation site is presented in red line. Right: Showing bands in the expected size (37 kDa) for the purified *RPS2 WT* and *C222S* mutant recombinant proteins. 12% SDS-PAGE gel stained with Coomassie blue or Western blot with RPS2 antibody. (F) Gel-based ABPP analysis of HEL against recombinant human *RPS2 WT* or *C222S* mutant proteins. Proteins were preincubated with DMSO vehicle or different concentrations of HEL before IA-rhodamine labeling. Proteins were resolved by SDS-PAGE and visualized by in-gel fluorescence, and protein loading was assessed by Coomassie staining. (G) MST traces and dose−response curves of labeled *RPS2 WT* or *C222S* mutant proteins bound with HEL. Error bars indicate the SD between the performed three technical replicates. Dissociation constants (K_D) are shown.

As shown in Fig. 4C, the median survival time of AML patients in the group with high expression levels of rRNA metabolic processes was significantly lower than that in the group with low expression levels ($P = 0.0034$). Taken together, the combined results of the transcriptomic GO enrichment analysis and GSEA potentially suggest that HEL inhibits *NPM1* mutant AML cells by disrupting rRNA processing and proteasome pathways.

To validate the screening results, we used northern blotting to analyze the effect of HEL on rRNA processing in OCI-AML3 cells. The RNA polymerase I inhibitor actinomycin D (ActD) was used as a positive control[39]. As shown in Fig. 4D and E, HEL significantly reduced the intracellular 30 S rRNA content ($P = 0.0024$) by inhibiting 47 S precursor rRNA shearing to 30 S rRNA in OCI-AML3 cells at a dose of 5 μmol/L.

The small ribosomal subunits mainly control the shearing of 47S into 30S rRNA precursors[40–43], suggesting that 5 μmol/L HEL disrupts the processing of RNA precursors by small ribosomal subunits, thereby blocking 30S rRNA biogenesis. At a dose of 10 μmol/L, 32S, 26S, 21S, 18S-E, and 12S rRNA processing was significantly blocked in treated cells compared to the control group ($P = 0.0013$, 0.049, 0.022, 0.002, and 0.0007, respectively), suggesting that at high doses (Fig. 4E), HEL causes severe damage to all ribosomal subunits. Processing of the above precursor rRNAs is necessary for the maturation of rRNAs (including 18S, 28S, and 5.8S), which further assemble into 40S and 60S ribosomal subunits that are translocated outside the nucleus to participate in the corresponding biological functions of ribosomes.

Disruption of rRNA processing leads to impairment of ribosome assembly, causing nucleolar stress[44–47]. The FBL protein can be used as a marker for nucleolar morphology[44]. As shown in Fig. 4F and Supporting Information S8A, at a dose of 5 μmol/L, HEL caused significant changes in the nucleolus morphology of OCI-AML3 and IMS-M2 cells, with typical features of nucleolus stress, such as nucleolus consolidation, dispersion, and disappearance. These cells showed significant increases in the positive rate of nucleolar stress after HEL

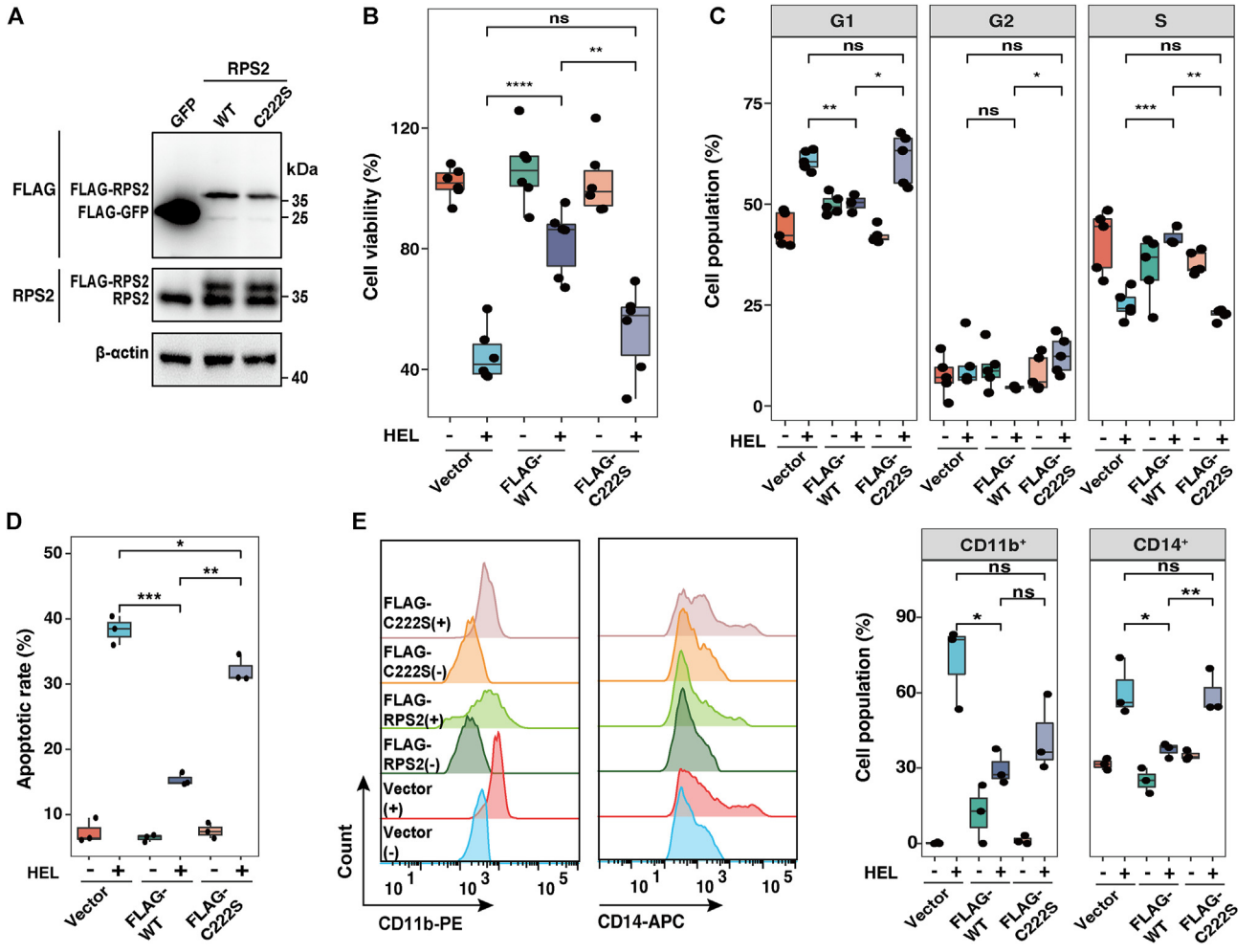

Figure 6 HEL impairs *NPM1* mutant AML cells and induces cell differentiation through targeting RPS2. (A) Anti-FLAG, anti-RPS2 and loading control anti-β-actin protein expression in OCI-AML3 cells stably expressing FLAG-GFP, FLAG-RPS2 WT or FLAG-RPS2 *C222S* mutant assessed using western blotting. (B)–(E) Cell viability (B, $n = 6$); cycles (C, $n = 5$), apoptotic rates (D, $n = 3$) and differentiation status (E, $n = 3$) of OCI-AML3 cells transiently expressing pcDNA3.1 vector, FLAG-RPS2 WT or a *FLAG-RPS2 C222S* mutant treated with DMSO or HEL (5 μmol/L) for 48 h, cell viability was tested by MTT method and cell cycle, apoptosis, and differentiation were all tested by flow cytometry method. Representative flow cytometry charts of experiments C&D are shown in Supporting Information Figs. S10 and S11. All the above experiments were analyzed by at least three biological replicates, presented as Median ± IQR; ns, not significant, $^{*}P < 0.05$, $^{**}P < 0.01$, $^{***}P < 0.001$, $^{****}P < 0.0001$.

treatment ($P < 0.001$, Fig. S8C). It has been reported that *NPM1* mutant AML cells are more sensitive to nucleolar stress than WT cells[7], which is associated with a shift in localization of NPM1c from the cytoplasm to the nucleus during nucleolar stress, thereby inhibiting the re-entry of *p53* oncoprotein into the nucleus and exerting AML inhibitory activity. Therefore, we determined the localization of the NPM1c protein before and after administration of HEL using confocal microscopy and found that HEL caused a shift in NPM1c protein localization from the cytoplasm to the nucleus including OCI-AML3 (Fig. 4G) and IMS-M2 (Fig. S8A) cells, which further validates that HEL causes significant nucleolar stress in NPM1 mutant AML cells. Further studies revealed that HEL did not affect the morphology of the nucleolus of the WT OCI-AML2 cells and the nuclear distribution of NPM1 at the same dose (Fig. S8B and S8C), which suggests the sensitivity of HEL on the rRNA processing pathway of the mutant cells.

It has been reported that the translocation and expression of NPM1c protein may somewhat regulate the binding of p53 and HDM2 proteins in NPM1 mutant AML cells, resulting in p53 accumulation, which may cause the corresponding anti-AML effect[48]. To verify whether HEL's anti-AML activity depends on this pathway, we used siRNA to knock down the expression of NPM1 in OCI-AML3 cells and observe HEL's activity in knockdown cells. The results are demonstrated in the Supporting Information Fig. S9, OCI-AML3 cells showed significant changes in cell proliferation inhibition ($P = 0.0032$), induction of apoptosis ($P = 0.0012$), G1 cell cycle arrest ($P = 0.0095$), cell differentiation ($P = 0.00017$ for $CD11b^+$ and $P = 0.00028$ for $CD14^+$) and p53 accumulation ($P = 0.05$) when NPM1 was knockdown by siRNA, which is consistent with the results reported by Balusu et al[49]. When HEL was administered in *NPM1* knockdown cells, the p53 accumulation, cell proliferation inhibition, apoptosis induction, G1 cell cycle arrest, and cell differentiation activities significantly elevated when compared with either non-drug administered *NPM1* knockdown or HEL-treated si*NC* control cells, which indicates that HEL's activity on *NPM1* mutant AML cells is not dependent on NPM1−HDM2−p53 pathway. Other protein targets on the Pre-rRNA processing pathway of AML cells need to be further investigated.

3.4. RPS2 is the primary target of HEL anti-NPM1 mutant AML and C222 is the covalent binding site

In accordance with previous results, we found that HEL inhibits rRNA metabolic processes by disrupting the function of pre-ribosomal subunits. However, it remains unclear which proteins are targeted. HEL contains covalent nucleophilic groups (among which the signature group is α-methylene-γ-butyrolactone), and we speculate that they may covalently interact with cysteine in target proteins.

We, therefore, used the QTRP technique[29] to screen for potential targets and sites for covalent binding with HEL. We labeled the blank and HEL-administered proteomic samples with the thiol-reactive probe IPM separately, followed by sample processing, mass spectrometry, and data analysis according to the literature (Fig. 5A).

As shown in Fig. 5B, human 40S ribosomal protein S2 (RPS2) was the main target for HEL binding in OCI-AML3 cells, and C222 was the main site for covalent binding. Experiments were performed in quartic, as shown in Supporting Information Table S4. The results of all four screens revealed that HEL binds covalently to position C222 of the RPS2 protein with $R_{H/L}$ values of 5.33, 9.12, 10.72 and 10.12, respectively, further validating the reproducibility of the QTRP screening results.

For the RPS2 protein, QTRP recognized a total of four cysteine-containing peptides, including C182, C188, C222, and C229, and the MS results shown in Fig. 5C suggest that the $R_{H/L}$ values of the peptides at positions C182, C188, and C229 were 1.16, 0.86, and 1.01, respectively (all less than 3.0), while only the $R_{H/L}$ value at position C222 was greater than 3.0 (9.12). This provides further evidence that position C222 is the likely site of covalent binding of HEL to the RPS2 protein.

Next, we examined whether the covalent binding of HEL to the C222 position of RPS2 changed with increasing concentrations of HEL. The results are shown in Fig. 5D. The covalent binding capacity of HEL to the RPS2 protein was significantly different when administered at a concentration of 10 μmol/L compared to 1 μmol/L ($P = 0.046$), although no significant change in the binding capacity of HEL to RPS2 was observed in OCI-AML3 cells between HEL concentrations of 10 and 50 μmol/L ($P = 0.70$), suggesting that the covalent binding capacity to the RPS2 protein becomes saturated when administered at concentrations >10 μmol/L.

To further validate the binding of HEL to RPS2, we designed a prokaryotic expression plasmid (pET28a-RPS2-WT) containing a sequence for human RPS2 protein sourced from NCBI (GeneID: 6187 NM_002952.4) and used a site-directed mutagenesis kit to change position 222 in the protein from cysteine to serine. The results of plasmid mutation sequencing are shown in Fig. 5E. The results of Coomassie blue staining and western blotting of RPS2 and its mutant recombinant proteins obtained by prokaryotic expression are shown in Fig. 5E.

We confirmed that RPS2 was a direct target of HEL using gel-based ABPP approaches; Fig. 5F shows that HEL competes against rhodamine-functionalized iodoacetamide (IA-rhodamine) labeling of recombinant human WT RPS2 protein in a dose-dependent manner. HEL bound to the C222S mutant RPS2 protein with a lower affinity than the WT protein, suggesting that C222 of RPS2 is the binding site of HEL.

We used MST experiments to evaluate the binding parameters of HEL with either WT or mutant RPS2 recombinant proteins. As shown in Fig. 5G, by curve fitting the changes in the MST signal of the interaction between HEL and RPS2 proteins, we obtained the equilibrium dissociation constant K_D values and found that the WT RPS2 binds to HEL with a K_D value of 3.05 μmol/L whereas the C222S mutant protein of RPS2 binds to HEL with a K_D value of 220.1 μmol/L. This further validated that HEL covalently targets the human RPS2 protein at site C222.

Validation of RPS2 as a target for HEL in the treatment of *NPM1* mutant AML was also performed at the cellular level. We designed a eukaryotic expression plasmid containing the RPS2 protein with a FLAG tag (pcDNA3.1-RPS2-FLAG) and mutated the cysteine at position 222 to serine, as described above. The plasmids were then transfected into OCI-AML3 cells, and as shown in Fig. 6A, the cells expressed the FLAG-tagged RPS2 proteins.

Next, we evaluated the effects of HEL administration on transfected cells, and as shown in Fig. 6B−E and Supporting Information Figs. S10 and S11, compared to the blank plasmid group (vector), the inhibition of OCI-AML3 cell proliferation was significantly reduced with wild-type *RPS2-FLAG* plasmid transfection ($P < 0.0001$), and its ability to induce cell apoptosis, cell G1 phase arrest, and cell differentiation were all significantly blocked ($P = 0.025$, 0.002, 0.032 for $CD11b^+$, and 0.041 for $CD14^+$, respectively). In contrast, after transfection with the *RPS2 C222S* mutant plasmid, no significant differences were observed

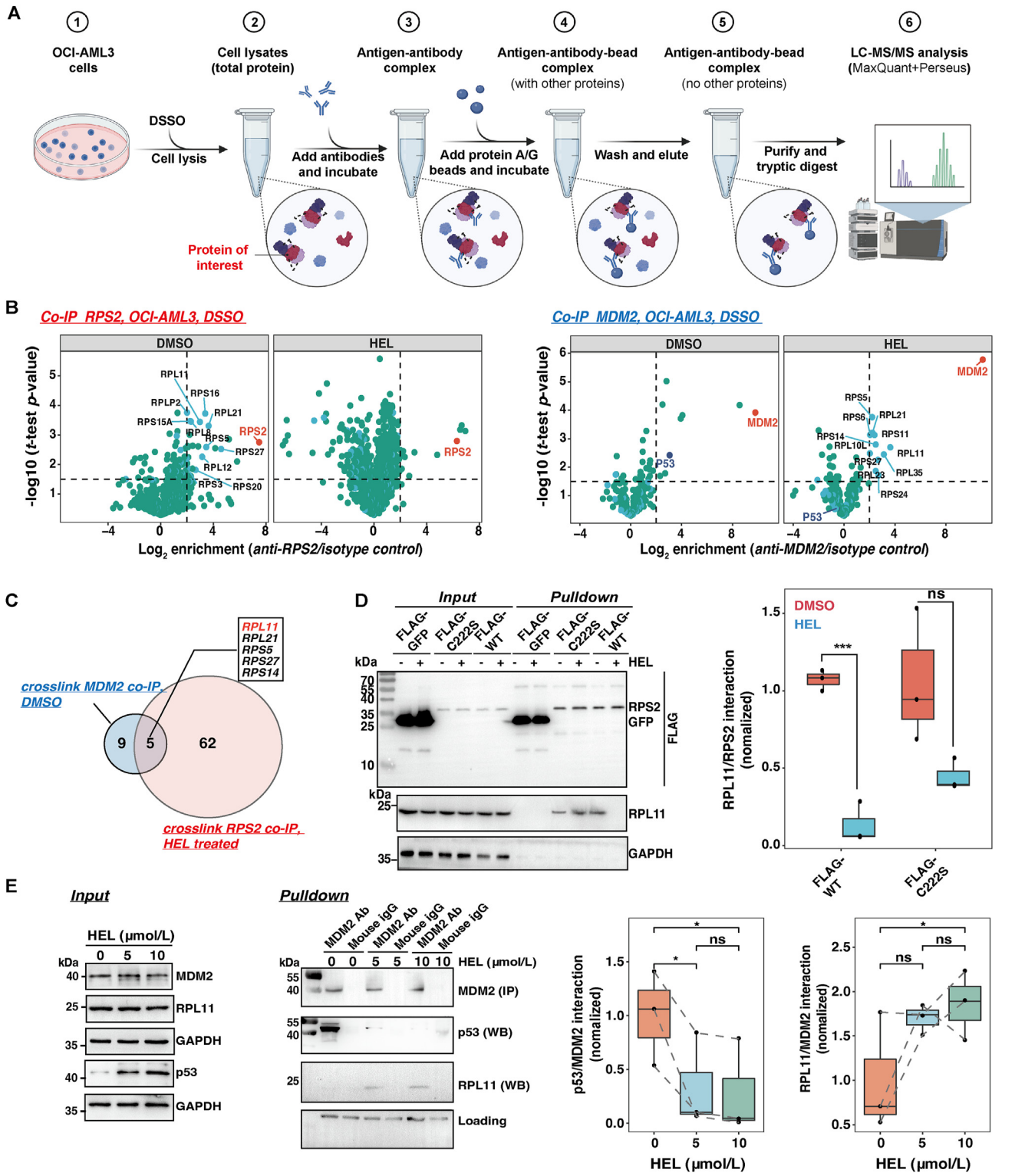

Figure 7 HEL inhibits RPS2 interaction with the ribosome proteins (RPs) therefore affecting the RPs−MDM2−p53 pathway. (A) Schematic workflow of MS-based Co-IP. OCI-AML3 cells were treated with 10 μmol/L HEL or DMSO, respectively, for 24 h. Subsequently, DSSO linker was added to covalently link protein complexes within cells. RPS2 (or MDM2) and linked proteins were enriched using an anti-RPS2 (or anti-MDM2) antibody immobilized on protein A/G beads. Tryptic peptides were measured *via* LC−MS/MS, and analyzed using MaxQuant and Perseus. (B) Volcano plots represent two-sample *t*-test results of anti-RPS2 Co-IP compared to isotype control Co-IP ($n = 3$). Cut-off criteria were defined as $\log_2 = 2$ (4-fold enrichment) enrichment factor and $-\log_{10}$ (*t*-test *P*-value) $= 1.5$ (dotted lines). RPS2 (or MDM2) is colored in red, RPs in blue and p53 in indigo. (C) Venn diagram showing the overlap between the anti-MDM2 Co-IP (DMSO treated) and anti-RPS2 Co-IP (HEL treated) enriched proteins. The common proteins are listed, where RPL11 (red) possess the highest enrichment score. (D) The OCI-AML3 cells stably expressing FLAG-GFP, FLAG-RPS2 WT or

in the proliferation, cell cycle arrest, and differentiation of OCI-AML3 cells caused by HEL as compared to the control plasmid (P = 0.28, 0.88, and 0.079 for $CD11b^+$ and 0.87 for $CD14^+$, respectively). Significant differences were also observed in proliferation, apoptosis, G1 phase cell cycle arrest, and cell differentiation of AML cells that were transfected with mutant plasmid compared to those with WT plasmid after HEL treatment (P = 0.003, 0.0014, 0.014 and 0.0027 for $CD14^+$, respectively). The above results further validated that HEL binds to C222 of RPS2 and that this binding affects the proliferation, apoptosis, cycle, and differentiation of OCI-AML3 cells.

3.5. *HEL affects the RPs−MDM2−p53 pathway, and anti-NPM1 mutant AML activity is dependent on p53*

As reported previously, the RPS2 protein is an important 40S ribosomal protein, and its main functions include ribosome assembly and the processing and maturation of pre-rRNAs[50,51]. To observe the role of RPS2 protein in *NPM1* mutant AML and its impact on downstream pathways, we first investigated the interactome of RPS2 protein in *NPM1* mutant AML cells using MS-based Co-IP experiments. Co-IP with anti-RPS2 antibody immobilized on magnetic beads was performed using DSSO cross-linking reagent, enabling the capture of transient binding proteins[34].

The protocols used are shown in Fig. 7A. The proteins captured by the RPS2 antibody were analyzed by LC−MS/MS. Compared with the isotype control, OCI-AML3 cells contained many significantly enriched proteins ($\log_{10}P > 1.5$, Log_2 enrichment >2) (Fig. 7B and Table S5), including a variety of ribosomal proteins (blue dots) that can bind to RPS2, such as RPL11, RPL21, and RPS5.

To determine the effect of HEL on the proteins that were found to bind to RPS2, Co-IP experiments were repeated 24 h after HEL treatment prior to DSSO cross-linking. As shown in Fig. 7B and Table S5, treatment with HEL reduced the number of ribosomal proteins bound to RPS2, suggesting HEL targets the RPS2 protein and disrupts the biogenesis of ribosomes in *NPM1* mutant AML cells, causing nucleolar stress and leading to the mutual disassembly of ribosomal proteins bound to RPS2.

Free-state ribosomal proteins further induce downstream biological activities. It has been reported that when cells experience nucleolar stress, numerous free-state ribosomal proteins in the nucleus bind competitively to MDM2 proteins, affecting the RPs−MDM2−p53 pathway and inhibiting the degradation of p53, thus affecting proliferation, the cell cycle, and differentiation[52,53]. Therefore, we analyzed the effect of HEL on MDM2-binding proteins using MS-based Co-IP. LC−MS/MS analysis of the proteins captured by the MDM2 antibody revealed that OCI-AML3 cells treated with HEL were significantly enriched in multiple ribosomal proteins (blue dots) compared to the control, and had a significant loss of p53 protein enrichment (purple dots), suggesting that HEL promotes the binding of free-state ribosomal proteins to MDM2 proteins, affecting the RPs−MDM2−p53 pathway, thereby freeing p53 protein (Fig. 7B and Table S6). In summary, five ribosomal proteins dissociated from RPS2 and bound to MDM2 after HEL administration, including RPL11, RPL21, RPS5, RPS27, and RPS14 (Fig. 7C).

Next, we validated the results of the MS-based Co-IP screening using western blotting. In the RPS2 pull-down assay (Fig. 7D), a significant amount of RPL11 was captured in FLAG-RPS2 expressing OCI-AML3 cells, indicating that RPS2 can bind to RPL11 in OCI-AML3 cells, which was significantly inhibited by HEL (P < 0.001). However, the binding inhibitory effect of HEL was not evident in cells expressing the FLAG-RPS2 C222S mutant protein.

The ribosomal proteins are reported to be key contributors that make up the pre-ribosomes and maintain the structure of the nucleolus, both of which are mainly distributed in the nucleus[52]. When HEL targets RPS2, resulting in free RPL11 transferred from the nucleus to the cytosol, where it can bind to MDM2 to generate downstream effects. The significant changes in the distribution of RPL11 protein from the nucleus to the cytoplasm after HEL treatment can further verify the results of the above Mass Co-IP experiments (Supporting Information Fig. S12).

In the protein pulldown assay with MDM2 (Fig. 7E), the binding of MDM2 to p53 was significantly decreased (P = 0.042), and correspondingly, its binding to the RPL11 was significantly increased (P = 0.044) after HEL administration. All the above results suggest that HEL affects the RPs−MDM2−p53 pathway in OCI-AML3 cells at the molecular level.

p53 plays a key role in the RPs−MDM2−p53 pathway[52,53]. To validate the essential role of *p53* in the physiological activity of HEL on OCI-AML3 cells, we constructed a p53 knockdown OCI-AML3 cell line. As shown in Fig. 8A−D and Figs. S13 and S14, knockdown of *p53* in OCI-AML3 cells significantly reduced the proliferation inhibitory activity of HEL in OCI-AML3 cells (P < 0.001), and significantly impaired the ability of HEL to induce apoptosis (P = 0.0003), arrest the cell cycle at the G1 phase (P = 0.023), and induce differentiation (P = 0.003 for $CD11b^+$, P = 0.002 for $CD14^+$). These results were further corroborated by Western blot analysis. The results in Fig. 8E and Supporting Information Fig. S15 show that the apoptosis-associated protein c-Cas3 was not significantly increased by HEL administration after *p53* knockdown, nor was the expression of cyclin p21 (cell cycle arrest-related protein) and CEBP/α (a protein related to cell differentiation) significantly increased by HEL administration. In summary, HEL modulates the RPs−MDM2−p53 pathway in OCI-AML3 cells by targeting the RPS2 protein, thereby exerting an inhibitory effect on the physiological activity of OCI-AML3 cells, which is dependent on the p53 protein.

3.6. *RPS2 is an essential target for NPM1 mutant AML treatment, and this target is p53-dependent*

To further understand the role of RPS2 protein in the treatment of *NPM1* mutant AML and to determine whether it is a suitable target

FLAG-RPS2 C222S were treated with DMSO or HEL (10 μmol/L) for 24 h, FLAG-GFP-, FLAG-RPS2-WT- and FLAG-RPS2-C222S-interacting proteins were subsequently enriched and subjected to Western blot analysis, protein levels of FLAG-tagged proteins, RPL11 and loading control GAPDH showing specific interaction of RPL11 with FLAG-RPS2 WT, however, when cells were treated with HEL, this interaction will be significantly reduced. Although the *C222S* mutant RPS2 protein can also specifically interact with RPL11, this interaction was not disrupted by HEL. (E) Western blot analysis of MDM2, p53 and RPL11 expression levels of OCI-AML3 either treated with DMSO or HEL (5 and 10 μmol/L) for 24 h and Co-IP of MDM2 in OCI-AML3 cells and detection of MDM2 and interactors p53/RPL11 by Western blot analysis. Gels shown in D and E are representative blots from n = 3 biologically dependent samples per group, bands were quantitated by ImageJ, presented as Median ± IQR; ns, not significant, *P < 0.05, **P < 0.01, ***P < 0.001.

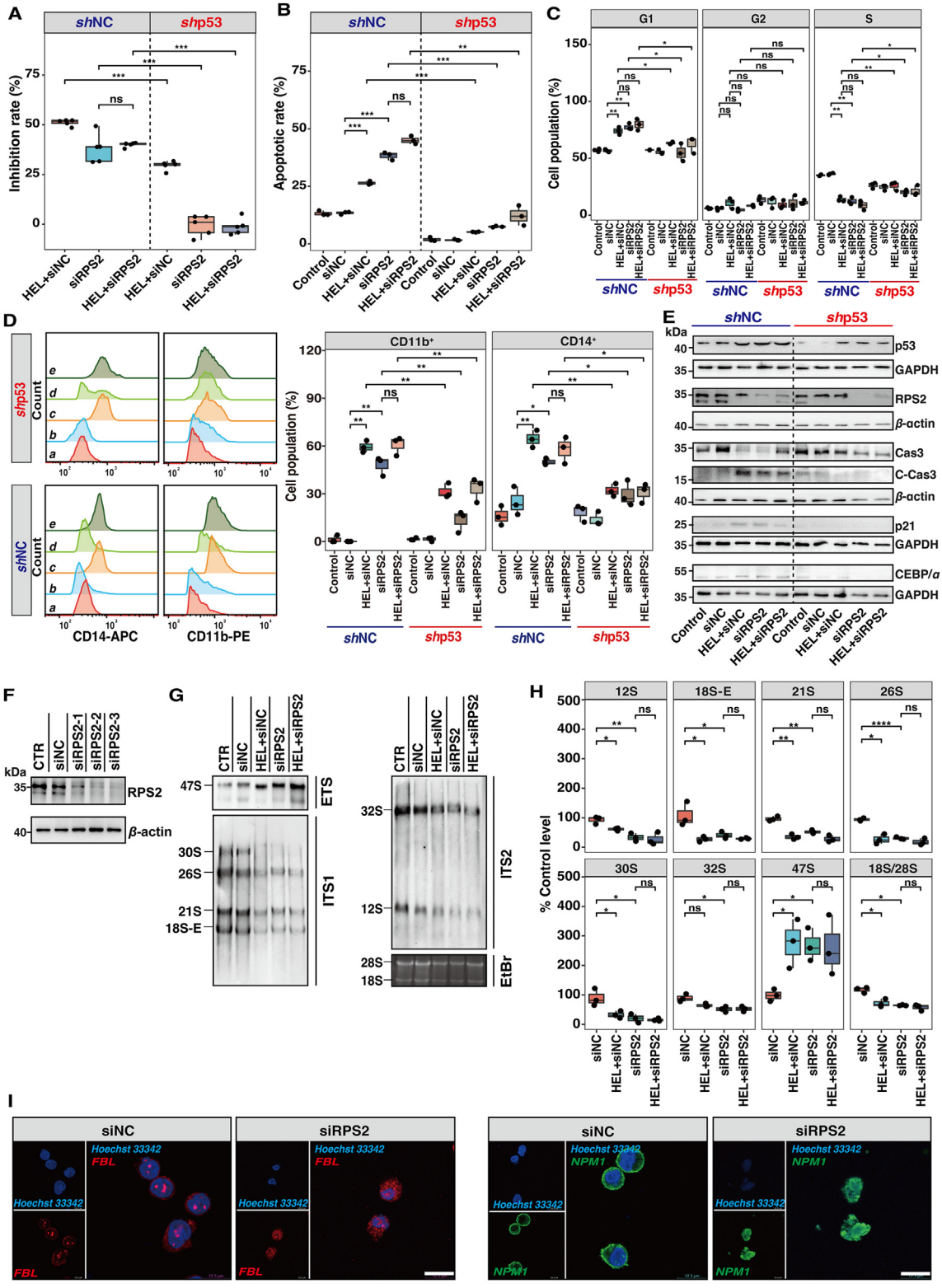

Figure 8 RPS2 is an essential target for *NPM1* mutant AML treatment, and this target is *p53* dependent. OCI-AML3 *sh*NC (blue) or *sh*p53 (red) cells transfected with RPS2 siRNA or si*NC* (control) and treated with DMSO or HEL (5 μmol/L), respectively for 48 h, the cells were then tested for the (A) proliferation, (B) apoptosis, (C) cycle arrest, and (D) differentiation status [a, DMSO; b, si*NC*; c, *HEL* (5 μmol/L)+si*NC*; d, si*RPS2*; e, *HEL* (5 μmol/L)+si*RPS2*] and (E) expressions of p53, RPS2, caspase 3, C-caspase 3, p21 and CEBP/*α* proteins. Experiments (A) was analyzed by five biological replicates; experiments (B−D) were analyzed by three biological replicates. Representative flow cytometry charts of experiments B&C are shown in Supporting Information Figs. S13 and S14. All data are presented as Median ± IQR; ns, not significant, $^{*}P < 0.05$, $^{**}P < 0.01$, unpaired *t* test; gels shown in experiment (E) are representative blots for three biological independent samples per group;

for treatment, we knocked down *RPS2* in OCI-AML3 cells by siRNA, as shown in Fig. 8F. Northern blotting was performed to analyze the effect of this protein on the processing of pre-rRNA in cells. As shown in Fig. 8G and H, siRNA knockdown of *RPS2* resulted in significant inhibition of 32S ($P = 0.018$), 30S ($P = 0.036$), 26S ($P < 0.0001$), 21S ($P = 0.002$), 18S-E ($P = 0.01$), and 12S ($P = 0.05$) pre-rRNAs and reduced the ratio of 28S/18S compared to that in the control group (si*NC*) ($P = 0.01$). This suggests that RPS2 is involved in pre-rRNA processing in OCI-AML3 cells.

No significant difference was observed in pre-rRNA processing in OCI-AML3 cells with *RPS2* knockdown after 48 h of HEL treatment compared to the non-drug administered RPS2 knockdown group, further suggesting that HEL mainly disrupts pre-rRNA synthesis in *NPM1* mutant AML cells by targeting the RPS2 protein.

Confocal microscopy observations indicated that, compared to controls, RPS2 gene knockdown resulted in significant changes in the structural morphology of OCI-AML3 nucleoli with typical features of nucleolar stress, which is consistent with results observed following administration of HEL (Fig. 8I). The NPM1 protein localization assay also suggested that the knockdown of *RPS2* resulted in a shift in the localization of the NPM1 protein from the cytoplasm to the nucleus (Fig. 8I). For *NPM1* mutant IMS-M2 cells, knockdown of RPS2 had the same effect on the nucleolus structure, producing significant nucleolus stress (Supporting Information Fig. S16A). The positive rates of cells with nucleolar stress after si*RPS2* transfection have been found both significantly increased in OCI-AML3 and IMS-M2 cells when compared with si*NC* group (Fig. S16C). In contrast, for WT OCI-AML2 cells, knockdown of RPS2 did not cause significant nucleolus structure changes (Fig. S16B) and showed a significantly lower rate of positive cells with nucleolar stress than mutant OCI-AML3 cells (Fig. S16C). The above results demonstrate that RPS2 is an essential protein that controls ribosomal biogenesis in *NPM1* mutant AML cells and thus affects nucleolar function.

In terms of cell physiology, knockdown of *RPS2* significantly inhibited cell proliferation ($P < 0.001$), induced apoptosis ($P = 0.001$), caused G1 cycle arrest ($P = 0.0024$), and led to a significant increase in the expression of the cell differentiation-associated protein $CD11b^+$ ($P = 0.01$) and $CD14^+$ ($P = 0.0064$), significantly elevated the p53 protein expression in OCI-AML3 cells ($P = 0.0071$) compared to the si*NC* control group (Fig. 8A−D and Supporting Information Fig. S17). The other *NPM1* mutant cell line, IMS-M2, showed consistent results with OCI-AML3, and knockdown of RPS2 protein also significantly inhibited cell proliferation ($P = 0.00013$), induced apoptosis ($P = 0.035$), arrested the cell cycle in the S phase ($P = 0.0019$), promoted cell differentiation ($P = 0.015$ for $CD11b^+$ and $P = 0.0026$ for $CD14^+$), and significantly elevated cellular p53 protein expression ($P = 0.001$). These effects, however, were not significant in *NPM1* WT OCI-AML2 cells (Fig. S17), which suggest that RPS2 may be an essential target for treating *NPM1* mutant AML.

When HEL was administered for 48 h after knockdown of *RPS2* in OCI-AML3 cells, these effects did not significantly differ from the non-drug administrated knockdown group, verifying that HEL disrupts the physiology of *NPM1* mutant AML cells mainly depending on the RPS2 protein. However, when *p53* was knocked down in OCI-AML3 cells, the proliferation inhibition, apoptosis induction, G1 phase cell cycle arrest, and $CD11b^+$ differentiation caused by *RPS2* knockdown were significantly reduced or lost ($P < 0.001$, $P < 0.001$, $P = 0.027$, and $P = 0.01$, respectively) when compared with the control group (*shNC*), suggesting that the effects of *RPS2* on *NPM1* mutant AML are dependent on p53 (Fig. 8A−D, Figs. S13 and S14). These findings were further confirmed by Western blot analysis of changes in the expression levels of proteins downstream of p53 (Fig. 8E and Fig. S15).

4. Discussion

Currently, *NPM1* is the most commonly mutated gene in AML patients, but there is a lack of targeted treatment options. Multiple clinical studies have reported that AML patients with *NPM1* mutations are prone to relapse. The XPO1 protein inhibitor Selinexor, which targets the nuclear export of the NPM1c protein, has recently been reported as a targeted therapy for this disease; however, it is still in the clinical trial phase[7−10].

Notably, in this study, we provided a novel natural sesquiterpene lactone lead compound for the treatment of *NPM1* mutant AML. The results of *in vitro* and *in vivo* experiments showed that *NPM1* mutant AML cells are sensitive to this lead compound, as it inhibits proliferation, induces apoptosis, causes cell cycle arrest in the G1 phase, and induces differentiation into normal blood cells.

Most importantly, through target pathway screening and validation, HEL was the first compound to be identified as a covalent inhibitor of the 40S ribosomal protein RPS2, which, when covalently bound to RPS2 at its C222 site, disrupts the processing of rRNA precursors and causes nucleolar stress in *NPM1* mutant AML cells. This, in turn, regulates the RPs−MDM2−p53 pathway and decreases the binding affinity between MDM2 and p53, thereby activating the p53 pathway and its downstream effects.

There are two current therapeutic options for the upregulation of ribosomal biogenesis driven by oncogenes in cancer[54]: first, the use of classical chemotherapeutic agents (*e.g.*, oxaliplatin, cisplatin, actinomycin D, and 5-FU) and poly ADP ribose polymerase (PARP) inhibitors, which cause DNA damage and inhibit ribosomal biogenesis in cells through a variety of mechanisms, thus inhibiting cell proliferation and inducing cell cycle arrest. However, the biggest disadvantages of these agents are their poor selectivity and genomic toxicity. Second, the use of newly discovered drugs that selectively target Pol I transcript activity, such as CX-5461, which has the advantages of good selectivity and low toxicity compared to the conventional chemotherapeutic drugs mentioned above, and now shows effects in a variety of

Protein level quantification results are shown in Supporting Information Fig. S15. (F) Expression of RPS2 protein and loading control actin levels in OCI-AML3 cells transfected with *RPS2* siRNA and siNC (control), assessed using Western blot. (G, H) Northern blot analysis of pre-rRNA processing phenotypes after transfected with *RPS2* siRNA or si*NC* (control) treated with DMSO or HEL (10 μmol/L) for 48 h, respectively. Mature rRNAs were shown on the EtBr-stained gel. Bands on the Northern blots or EtBr gels ($n = 3$) were quantitated by ImageJ, presented as Median ± IQR; ns, not significant, $^*P < 0.05$, $^{**}P < 0.01$, $^{****}P < 0.0001$. (I) FBL (red) and NPM1 (green) localization in the *RPS2* knockdown OCI-AML3 cells by IF. Hoechst 33342 (blue) was used to stain for nuclei. Images by Leica SP8 confocal microscope. Scale bar, 12.3 μm. Quantification of percentage of cells with nucleolar stress is shown in Supporting Information Fig. S16.

preclinical cancer models without significant genotoxicity[55]. However, the compound is still in clinical or preclinical studies for cancer treatment, and there are still some bioavailability and solubility issues; therefore, the utility of the compound as a drug is still unknown.

Currently, there are no targeted inhibitors of ribosomal proteins. The finding that HEL inhibits the covalent binding of RPS2 in this study opens a new field for the development of drugs targeting the overexpressed ribosome biogenesis pathway in AML. In addition, it has been reported that solid tumors other than AML, such as breast cancer and melanoma, cause abnormal overexpression of the ribosomal biogenesis pathway[56]. Therefore, the efficacy of HEL in the treatment of solid tumors should be further evaluated.

Through bioinformatic analysis of clinical data, we found that pathways associated with rRNA metabolism, preribosome, and ribosomal biogenesis were significantly upregulated in AML patients with *NPM1* mutations pathways and that patients with activated preribosome and rRNA metabolic pathways showed poor prognosis. It is widely accepted that the NPM1 protein plays a crucial role in the regulation of ribosomal biogenesis in cells, but the mechanism underlying ribosomal biosynthesis and rRNA processing pathway in mutated variants of this protein is unclear. It has been suggested that the non-coding long RNA HOXB-AS3 interacts with ErbB3-binding protein 1 (EBP1) and directs it to the ribosomal DNA site[57]. Through this mechanism, HOXB-AS3 can positively regulate rRNA transcription. Therefore, overexpression of HOXB-AS3 caused by *NPM1* mutations leads to the upregulation of rRNA processing and ribosomal biogenesis pathways in AML cells. However, this may be a reason for the significant upregulation of the ribosomal pathways due to *NPM1* mutation, and the underlying mechanism requires further investigation.

In the present study, we found that RPS2 is an important protein that regulates ribosomal biosynthesis and rRNA processing, and knocking down this protein significantly affects ribosomal synthesis, influences the RPs−MDM2−p53 pathway, and stabilizes p53 in *NPM1*-mutant AML cells. This leads to p53 pathway activation, resulting in proliferation inhibition, induction of apoptosis, cell cycle arrest, and cell differentiation. The above results suggest that RPS2 may be a new target for the treatment of *NPM1* mutant AML, but the mechanism underlying its effect on this disease remains to be verified by further in-depth experiments. On this basis, small-molecule drugs can be further developed to provide new targeted therapeutic options for patients suffering from similar diseases.

Acknowledgments

This work was supported by grants from the National Natural Science Foundation of China (82074067), Natural Science Foundation of Jiangsu Province China (BK20181419, China) and Natural Foundation of Jiangsu Higher Education Institutions of China (19KJA310006).

Author contributions

Xinzhi Wang designed experiments and obtained funding. Yin Feng, Yefan Han, Anni Hu, Yi Qu and Xinzhi Wang carried out experiments and analyzed the data. Yili Hu assisted in performing the flow cytometry experiments. Xinzhi Wang, Yin Feng and Yefan Han wrote the manuscript. Hao Wu, Li He reviewed/commented on the manuscript.

Conflicts of interest

The authors have no conflicts of interest to declare.

Appendix A. Supporting information

Supporting data to this article can be found online at https://doi.org/10.1016/j.apsb.2022.10.018.

References

1. Dohner H, Weisdorf DJ, Bloomfield CD. Acute myeloid leukemia. *New Engl J Med* 2015;**373**:1136−52.
2. Papaemmanuil E, Gerstung M, Bullinger L, Gaidzik VI, Paschka P, Roberts ND, et al. Genomic classification and prognosis in acute myeloid leukemia. *New Engl J Med* 2016;**374**:2209−21.
3. Kantarjian H, Kadia T, DiNardo C, Daver N, Borthakur G, Jabbour E, et al. Acute myeloid leukemia: current progress and future directions. *Blood Cancer J* 2021;**11**:41.
4. Kantarjian HM, Kadia TM, DiNardo CD, Welch MA, Ravandi F. Acute myeloid leukemia: treatment and research outlook for 2021 and the MD Anderson approach. *Cancer* 2021;**127**:1186−207.
5. Carter JL, Hege K, Yang J, Kalpage HA, Su YW, Edwards H, et al. Targeting multiple signaling pathways: the new approach to acute myeloid leukemia therapy. *Signal Transduct Target Ther* 2020;**5**:288.
6. Brown P, McIntyre E, Rau R, Meshinchi S, Lacayo N, Dahl G, et al. The incidence and clinical significance of nucleophosmin mutations in childhood AML. *Blood* 2007;**110**:979−85.
7. Falini B, Brunetti L, Sportoletti P, Martelli MP. NPM1-mutated acute myeloid leukemia: from bench to bedside. *Blood* 2020;**136**:1707−21.
8. Hoffmann H, Thiede C, Glauche I, Kramer M, Rollig C, Ehninger G, et al. The prognostic potential of monitoring disease dynamics in NPM1-positive acute myeloid leukemia. *Leukemia* 2019;**33**:1531−4.
9. Heath EM, Chan SM, Minden MD, Murphy T, Shlush LI, Schimmer AD. Biological and clinical consequences of *NPM1* mutations in AML. *Leukemia* 2017;**31**:798−807.
10. Brunetti L, Gundry MC, Sorcini D, Guzman AG, Huang YH, Ramabadran R, et al. Mutant *NPM1* maintains the leukemic state through HOX expression. *Cancer Cell* 2018;**34**:499−512.
11. Rolnik A, Olas B. The plants of the *Asteraceae* family as agents in the protection of human health. *Int J Mol Sci* 2021;**22**:3009.
12. Spring O. Sesquiterpene lactones from *Helianthus tuberosus*. *Phytochemistry* 1991;**30**:519−22.
13. Yuan XY, Cheng MC, Gao MZ, Zhuo RJ, Zhang LX, Xiao HB. Cytotoxic constituents from the leaves of Jerusalem artichoke (*Helianthus tuberosus* L.) and their structure−activity relationships. *Phytochem Lett* 2013;**6**:21−5.
14. Pan L, Sinden MR, Kennedy AH, Chai H, Watson LE, Graham TL, et al. Bioactive constituents of *Helianthus tuberosus* (Jerusalem artichoke). *Phytochem Lett* 2009;**2**:15−8.
15. Spring O, Schilling EE. The sesquiterpene lactone chemistry of *Helianthus* sect. *Atrorubentes* (Asteraceae: Heliantheae). *Biochem Syst Ecol* 1991;**19**:59−79.
16. Shin M, McGowan A, DiNatale GJ, Chiramanewong T, Cai TY, Connor RE. Hsp72 is an intracellular target of the alpha, beta-unsaturated sesquiterpene lactone, parthenolide. *Acs Omega* 2017;**2**:7267−74.
17. Grafakou ME, Barda C, Karikas GA, Heilmann J, Skaltsa H. Cajamolides A−N: cytotoxic and anti-inflammatory sesquiterpene lactones from Calea jamaicensis. *Bioorg Chem* 2021;**116**:105351.
18. Quintana J, Estevez F. Recent advances on cytotoxic sesquiterpene lactones. *Curr Pharm Design* 2018;**24**:4355−61.
19. Formisano C, Sanna C, Ballero M, Chianese G, Sirignano C, Rigano D, et al. Anti-inflammatory sesquiterpene lactones from *Onopordum illyricum* L. (Asteraceae), an Italian medicinal plant. *Fitoterapia* 2017;**116**:61−5.

20. Matsumoto T, Nakashima S, Nakamura S, Hattori Y, Ando T, Matsuda H. Inhibitory effects of cynaropicrin and related sesquiterpene lactones from leaves of artichoke (*Cynara scolymus* L.) on induction of iNOS in RAW264.7 cells and its high-affinity proteins. *J Nat Med* 2021;**75**:381−92.
21. Puente V, Laurella LC, Spina RM, Lozano E, Martino VS, Sosa MA, et al. Primary targets of the sesquiterpene lactone deoxymikanolide on *Trypanosoma cruzi*. *Phytomed* 2019;**56**:27−34.
22. Valkute TR, Aratikatla EK, Gupta NA, Ganga S, Santra MK, Bhattacharya AK. Synthesis and anticancer studies of Michael adducts and Heck arylation products of sesquiterpene lactones, zaluzanin D and zaluzanin C from *Vernonia arborea*. *RSC adv* 2018;**8**:38289−304.
23. Jakobs A, Steinmann S, Henrich SM, Schmidt TJ, Klempnauer KH. Helenalin acetate, a natural sesquiterpene lactone with anti-inflammatory and anti-cancer activity, disrupts the cooperation of CCAAT box/enhancer-binding protein β (C/EBPβ) and co-activator p300. *J Biol Chem* 2016;**291**:26098−108.
24. Wang XZ, Feng Y, Han YF, Wu H, inventors. *Nanjing University of Chinese Medicine, assignee. Sesquiterpene lactones and their medicinal derivatives of Helianthus tuberosus and their applications in the treatment of acute myeloid leukemia*. 2021 Dec 11. China patent CN No. 202111511412.8.
25. Backus KM, Correia BE, Lum KM, Forli S, Horning BD, Gonzalez-Paez GE, et al. Proteome-wide covalent ligand discovery in native biological systems. *Nature* 2016;**534**:570−4.
26. Isobe Y, Okumura M, McGregor LM, Brittain SM, Jones MD, Liang XY, et al. Manumycin polyketides act as molecular glues between UBR7 and P53. *Nat Chem Biol* 2020;**16**:1189−98.
27. Luo M, Spradlin JN, Boike L, Tong BQ, Brittain SM, McKenna JM, et al. Chemoproteomics-enabled discovery of covalent RNF114-based degraders that mimic natural product function. *Cell Chem Biol* 2021;**28**:559−66.
28. Dubiella C, Pinch BJ, Koikawa K, Zaidman D, Poon E, Manz TD, et al. Sulfopin is a covalent inhibitor of Pin1 that blocks Myc-driven tumors *in vivo*. *Nat Chem Biol* 2021;**17**:954−63.
29. Fu L, Li ZM, Liu KK, Tian CP, He JX, He JY, et al. A quantitative thiol reactivity profiling platform to analyze redox and electrophile reactive cysteine proteomes. *Nat Protoc* 2020;**15**:2891−919.
30. Streit S, Michalski CW, Erkan M, Kleeff J, Friess H. Northern blot analysis for detection and quantification of RNA in pancreatic cancer cells and tissues. *Nat Protoc* 2009;**4**:37−43.
31. Mansour FH, Pestov DG. Separation of long RNA by agarose-formaldehyde gel electrophoresis. *Anal Biochem* 2013;**441**:18−20.
32. Kok BP, Ghimire S, Kim W, Chatterjee S, Johns T, Kitamura S, et al. Discovery of small-molecule enzyme activators by activity-based protein profiling. *Nat Chem Biol* 2020;**16**:997−1005.
33. Entzian C, Schubert T. Studying small molecule-aptamer interactions using MicroScale Thermophoresis (MST). *Methods* 2016;**97**:27−34.
34. O'Reilly FJ, Rappsilber J. Cross-linking mass spectrometry: methods and applications in structural, molecular and systems biology. *Nat Struct Mol Biol* 2018;**25**:1000−8.
35. Kirsch VC, Orgler C, Braig S, Jeremias I, Auerbach D, Muller R, et al. The cytotoxic natural product vioprolide a targets nucleolar protein 14, which is essential for ribosome biogenesis. *Angew Chem Int Edit* 2020;**59**:1595−600.
36. Swords RT, Perez A, Rodriguez A, Watts JM, Schenk T, Vargas F, et al. In acute myeloid leukemia (AML), targeting the histone methyltransferase EZH2 promotes differentiation, impairs clonogenic survival and augments the anti-leukemic effects of the retinoid, all-*trans*-retinoic acid (ATRA). *Blood* 2015;**126**:460.
37. Zhang Z, Lu Y, Qi Y, Xu Y, Wang S, Chen F, et al. CDK19 regulates the proliferation of hematopoietic stem cells and acute myeloid leukemia cells by suppressing p53-mediated transcription of p21. *Leukemia* 2022;**36**:956−69.
38. Seipel K, Marques MT, Bozzini MA, Meinken C, Mueller BU, Pabst T. Inactivation of the p53−KLF4−CEBPA axis in acute myeloid leukemia. *Clin Cancer Res* 2016;**22**:746−56.
39. Perry RP, Kelley DE. Inhibition of RNA synthesis by actinomycin D: characteristic dose−response of different RNA species. *J Cell Physiol* 1970;**76**:127−39.
40. Robledo S, Idol RA, Crimmins DL, Ladenson JH, Mason PJ, Bessler M. The role of human ribosomal proteins in the maturation of rRNA and ribosome production. *RNA* 2008;**14**:1918−29.
41. Lessard F, Brakier-Gingras L, Ferbeyre G. Ribosomal proteins control tumor suppressor pathways in response to nucleolar stress. *Bioessays* 2019;**41**:1800183.
42. O'Donohue MF, Choesmel V, Faubladier M, Fichant G, Gleizes PE. Functional dichotomy of ribosomal proteins during the synthesis of mammalian 40S ribosomal subunits. *J Cell Biol* 2010;**190**:853−66.
43. Tafforeau L, Zorbas C, Langhendries JL, Mullineux ST, Stamatopoulou V, Mullier R, et al. The complexity of human ribosome biogenesis revealed by systematic nucleolar screening of pre-rRNA processing factors. *Mol Cell* 2013;**51**:539−51.
44. Henras AK, Plisson-Chastang C, O'Donohue MF, Chakraborty A, Gleizes PE. An overview of pre-ribosomal RNA processing in eukaryotes. *Wiley Interdiscip Rev RNA* 2015;**6**:225−42.
45. Yang K, Yang J, Yi J. Nucleolar Stress: hallmarks, sensing mechanism and diseases. *Cell Stress* 2018;**2**:125−40.
46. Turi Z, Lacey M, Mistrik M, Moudry P. Impaired ribosome biogenesis: mechanisms and relevance to cancer and aging. *Aging (Albany NY)* 2019;**11**:2512−40.
47. Nicolas E, Parisot P, Pinto-Monteiro C, de Walque R, De Vleeschouwer C, Lafontaine DLJ. Involvement of human ribosomal proteins in nucleolar structure and p53-dependent nucleolar stress. *Nat Commun* 2016;**7**:11390.
48. Kurki S, Peltonen K, Latonen L, Kiviharju TM, Ojala PM, Meek D, et al. Nucleolar protein NPM interacts with HDM2 and protects tumor suppressor protein p53 from HDM2-mediated degradation. *Cancer Cell* 2004;**5**:465−75.
49. Balusu R, Fiskus W, Rao R, Chong DG, Nalluri S, Mudunuru U, et al. Targeting levels or oligomerization of nucleophosmin 1 induces differentiation and loss of survival of human AML cells with mutant NPM1. *Blood* 2011;**118**:3096−106.
50. Ferreira-Cerca S, Pöll G, Gleizes PE, Tschochner H, Milkereit P. Roles of eukaryotic ribosomal proteins in maturation and transport of pre-18S rRNA and ribosome function. *Mol Cell* 2005;**28**:263−75.
51. Landry-Voyer AM, Bergeron D, Yague-Sanz C, Baker B, Bachand F. PDCD2 functions as an evolutionarily conserved chaperone dedicated for the 40S ribosomal protein uS5 (RPS2). *Nucleic Acids Res* 2020;**48**:12900−16.
52. Liu Y, Deisenroth C, Zhang YP. RP-MDM2-p53 pathway: linking ribosomal biogenesis and tumor surveillance. *Trends Cancer* 2016;**2**:191−204.
53. Mahata B, Sundqvist A, Xirodimas DP. Recruitment of RPL11 at promoter sites of *p53*-regulated genes upon nucleolar stress through NEDD8 and in an Mdm2-dependent manner. *Oncogene* 2012;**31**:3060−71.
54. Kang J, Brajanovski N, Chan KT, Xuan JC, Pearson RB, Sanij E. Ribosomal proteins and human diseases: molecular mechanisms and targeted therapy. *Signal Transduct Target Ther* 2021;**6**:323−45.
55. Drygin D, Lin A, Bliesath J, Ho CB, O'Brien SE, Proffitt C, et al. Targeting RNA polymerase I with an oral small molecule CX-5461 inhibits ribosomal RNA synthesis and solid tumor growth. *Cancer Res* 2011;**71**:1418−30.
56. Sulima SO, Hofman IJF, De Keersmaecker K, Dinman JD. How ribosomes translate cancer. *Cancer Discov* 2017;**7**:1069−87.
57. Papaioannou D, Petri A, Dovey OM, Terreri S, Wang E, Collins FA, et al. The long non-coding RNA HOXB-AS3 regulates ribosomal RNA transcription in NPM1-mutated acute myeloid leukemia. *Nat Commun* 2019;**10**:1−15.